BÚSQUEDA DE PARTÍCULAS DE LARGA VIDA EN EL LHC

(Search for Long-Lived Particles at the LHC)

Trabajo de Fin de Máster
para acceder al

MÁSTER INTERUNIVERSITARIO (UC-UIMP) EN FÍSICA DE PARTÍCULAS Y DEL COSMOS

Autor: Laura V. Trujillo Taborda

Director\es: Jesús Manuel Vizán García

Septiembre- 2020

FACULTAD DE CIENCIAS

Search for Long Lived Particles at the LHC
(Búsqueda de Partículas de Larga Vida en el LHC)

Author:
Laura TRUJILLO TABORDA

Supervisor:
Jesús Manuel VIZÁN GARCÍA

A thesis submitted in fulfillment of the requirements for the degree of

Master in Particle Physics and the Cosmos
(UC-UIMP)

September 18, 2020

Declaration of Authorship

I, Laura TRUJILLO TABORDA, declare that this thesis titled, "Search for Long Lived Particles at the LHC" and the work presented in it are my own. I confirm that:

- This work was done wholly or mainly while in candidature for a research degree at this University.
- Where any part of this thesis has previously been submitted for a degree or any other qualification at this University or any other institution, this has been clearly stated.
- Where I have consulted the published work of others, this is always clearly attributed.
- Where I have quoted from the work of others, the source is always given. With the exception of such quotations, this thesis is entirely my own work.
- I have acknowledged all main sources of help.
- Where the thesis is based on work done by myself jointly with others, I have made clear exactly what was done by others and what I have contributed myself.

Signed: 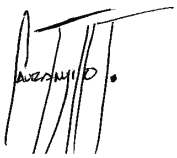

Date: September 18, 2020

UNIVERSIDAD DE CANTABRIA

Abstract

Master in Particle Physics and the Cosmos

Search for Long Lived Particles at the LHC

Given an observation of the Higgs boson with a mass of 125 GeV in the Large Hadron Collider (LHC) Run 1, a detailed study has been conducted on its properties, with numerous searches for new particles, resulting in no evidence of new Physics or significant deviations to predictions of the Standard Model (SM). Nonetheless, and despite the great success of the SM to describe an enormous range of physical phenomena; diverse theoretical considerations, such as challenges with SM to explain the mass of the Higgs boson taking into consideration its quantum corrections (hierarchy problem) motivate the search for Physics beyond the SM both by way of Run 2 LHC data analysis and of Run 3 in the period of high luminosity of the LHC.

In this context, it is important to propose that the absence of evidence of Physics beyond the SM can be explained due to the fact that it manifests in way of less common signatures in the LHC, being one of the most attractive options its materialization by way of new displaced particles. The objective of this research is to study this type of searches where long lived particles disintegrate, opening the way to pairs of charged and displaced leptons (muons and electrons).

The paper will focus on an ongoing advanced analysis of this type, which includes all Run 2 data of the LHC in the CMS experiment, with the purpose to explore the improvement of these searches in diverse situations. Diverse options can be explored: optimizations for signals with displacement not excessively preeminent, improvement of the efficiency of signal reconstruction or improvement of background estimations. The aspects in which this comes into play will depend primarily in the cumulative experience of research development at the start of the final Master project.

Keywords: Long-lived Particles, CMS experiment, LHC, high-energy physics, Beyond Standard Model, data analysis.

UNIVERSIDAD DE CANTABRIA

Resumen

Máster en Física de Partículas y del Cosmos

Búsqueda de Partículas de Larga Vida en el LHC

Desde la observación del bosón de Higgs con una masa de 125 GeV en el Run 1 del Large Hadron Collider (LHC) se han estudiado en detalle sus propiedades y se han llevado a cabo numerosas búsquedas de nuevas partículas, sin encontrarse evidencias de nueva Física ni desviaciones significativas a las predicciones del Modelo Estándar (ME). Sin embargo y a pesar del enorme éxito del ME para describir un enorme rango de fenómenos físicos, diversas consideraciones teóricas, tales como los problemas del ME para explicar la masa del bosón de Higgs teniendo en cuenta las correcciones cuánticas a la misma (problema de jerarquía), motivan la búsqueda de Física más allá del ME tanto mediante el análisis de datos del Run 2 del LHC como en el futuro Run 3 y en el período de alta luminosidad del LHC.

En este contexto, es importante plantearse que la ausencia de evidencias de Física más allá del Modelo Estándar puede deberse a que ésta se manifiesta en forma de signaturas menos habituales del LHC, siendo uno de las opciones más atractivas su materialización en forma de nuevas partículas desplazadas. El objetivo del presente trabajo es el estudio de este tipo de búsquedas donde las partículas de larga vida media se desintegran dando lugar a pares de leptones cargados (muones y electrones) desplazados.

El trabajo se basará en un análisis en marcha y avanzado de este tipo, el cual emplea el total de datos del Run 2 del LHC en el experimento CMS, para explorar la mejora de estas búsquedas en diversas situaciones.Diversas opciones pueden ser exploradas: optimizaciones para señales con desplazamiento no excesivamente prominente,mejora de la eficiencia de reconstrucción de señales, o mejoras en la estimación de fondos. Los aspectos en los que se incidirá principalmente dependerán de la experiencia acumulada en el trabajo en desarrollo de inicio del proyecto de fin de Máster.

Palabras Claves: Partículas de larga vida, experimento CMS, LHC, física de altas energías, física más allá del Modelo Estándar, análisis de datos.

Acknowledgements

Firstly, I would like to sincerely thank my supervisor Jesús for all the time he dedicated through the development of the present work as well as for sharing all his insightful comments and experience that allow me to grasp a better understanding of High Energy Physics and data analysis. I, also, would like to thank *Fundación Carolina* for giving me the opportunity to study abroad and funding my master degree.

Many thanks to my classmates, in particular, to Clara for showing me the remarkable spanish *cuisine* and the endless side of Cantabria together with sharing surreal and fascinating stories that made the lockdown disappear; and to Roaa, for our many discussions and insightful talks about science, theology, life and culture; it truly shows me how crucial it is to stand firm with and persevere to uphold your principles.

I have nothing but gratitude to my family, without whom I would not be here. My parents, who dedicated their time, hard work and unconditional support to encourage me on pursuing my goals; my achievements are indeed the result of their effort and sacrifice. My grandparents, who taught me all the things that one can not simply learn from books. And Dayra, whose perseverance and tenacity are a daily example for me, thank you for always wanted to be of help.

Last, but not least, I am very grateful to my friends who supported me throughout this year: Arturo, for always been there; Paula and Oscar, for all our *tintos* and advice; and Camila, for always having the right words. Thank you, guys for all the support and patience, as Milan Kundera once put it, loyalty to a friend is truly a virtue.

Contents

List of Figures

List of Tables

Chapter 1

Introduction

Particles with long lifetimes are predicted in many extensions of the Standard Model as a way to address series of still open questions suchlike the hierarchy problem, dark matter and neutrino masses. Even though the Standard Model has been quite successful in describing the behavior of fundamental particles; there are, however, pieces of the puzzle that are missing and that raise doubts on what is yet to be discovered. This motivates the quest for physics beyond the Standard Model, where Long-Lived Particles (LLP) emerge as a natural explanation on scenarios such as Supersymmetry (SUSY), RPV Supersymmetry, "hidden valleys" models and extended Higgs sectors.

The experimental signatures of LLP have captivated special attention, since the search of new particles with promptly signatures have yielded no results and LLP could manifest themselves through delayed decays. In other words, LLP signatures could be "hidden" in the detectors as stopped particles that decay out of time with collisions, having displaced vertices in the tracker or muon detectors. Such atypical signatures are subject of current study at LHC and could offer a plausible hint on the discovery of new physics at high-energies.

In particular, the LLP of interest in the given analysis is a spinless boson X that decays to final states that include a pair of charged leptons (electrons and muons), where the X boson is pair-produced in the decay of non-SM Higgs boson ($H \to XX$, $X \to l^+l^-$) [1].

This study is based on an ongoing analysis of searches for long-lived particles that decay into final states containing displaced leptons in the Run 2 of the LHC, using 2016 data collected with the CMS detector in proton proton collisions at $\sqrt{s} = 13$ TeV and it focuses on generated signal samples produced with `PYTHIA v8`, which benchmark model is BSM $H \to XX, 2\mu 2e$, where the mass for the Higgs boson is set to be 400 GeV, for the X boson 50, 150 GeV with mean proper lifetime τ, such as $c\tau = 4, 40, 400$ mm. The aim of the following study is to provide an estimation of the number of signal events in a sample using exclusively generation level information, in a way that could help to optimize cuts at analysis level and, additionally, to compare the performance between two algorithms for muon reconstruction: Muon Run 1-like and Displaced Global Muon Run 2-like algorithms.

The thesis is organized as follows: Chapter 2 provides a shortly introduction of the Standard Model together with extensions of the Standard Model with LLP; in Chapter 3 a review of the Large Hadron Collider and the CMS experiment is presented; while in Chapter 4 a briefly description on the different reconstruction algorithms is given; and in Chapter 5 the results obtained are illustrated and further discussed. Finally, the conclusions of the given analysis are presented in Chapter 6.

Chapter 2

Theoretical Introduction

The main goal of high-energy physics is to provide an effective mathematical description of the fundamental constituents of matter and the interactions between them. The known interactions are reduced to four forces: Strong interaction, electromagnetism, weak interaction and gravity. Although the electromagnetic and gravitational forces were somehow understood by classical physics, the growing understanding of quantum mechanics suggested that forces are transmitted through the interchange of particles. Also, the phenomenological description of β and α-decays allowed to depict properties of new short-ranged interactions, nowadays known as weak and strong forces. All that advances have lead to a more complete picture of the interactions involved between particles. On the other hand, elementary particles are so far described as excitations of quantum fields, which their behavior and mathematical framework is explained by the Quantum Field Theory (QFT) founded by Dirac[2], Pauli, Jordan [3] and Heisenberg [4].

The collection of mathematical expressions that coherently portrays three out of four fundamental interactions in nature (electromagnetic, weak and strong forces) and provides a way to classify elementary particles, is refer as the *Standard Model* (SM) of particle physics. However, despite the high precision of predictions provided by the SM in experimental studies, there are still limitations that pops up questions about the current understanding of the Universe such as: the hierarchy problem, the baryon asymmetry, the origin of neutrino masses and so on. Particularly, Some of many theories and models that are trying to elucidate answers for the apparently inconsistencies, involve particles with long lifetimes. In this chapter, a brief introduction for both the SM and its limitations along with extensions of the SM involving Long Lived Particles (LLP) is given.

2.1 Standard Model

In the 1960s, a theory explaining the unification between the weak and the electromagnetic interaction was proposed by Glashow [5], Weinberg [6] and Salam [7]. The empirical confirmations on neutral currents[1] and charged-current scattering[2] of such theory along with the Quantum Chromodynamics theory (QCD) gave rise to what is today called the *Standard Model* of particle physics.

Basically, the SM is a relativistic quantum field theory (QFT), which fundamental foundation is symmetry. The SM comes from the principle of local gauge invariance and thus, it suggests that interactions of vector bosons are associated with a global symmetry group [10]. The description of the three interactions mentioned above is based on the group of symmetries $SU(3)_C \otimes SU(2)_L \otimes U(1)_Y$.

[1] see *Neutrino Scattering at CERN* (Block,1964)[8]
[2] see *Gargamelle experiment at CERN* (Hasert,1974)[9]

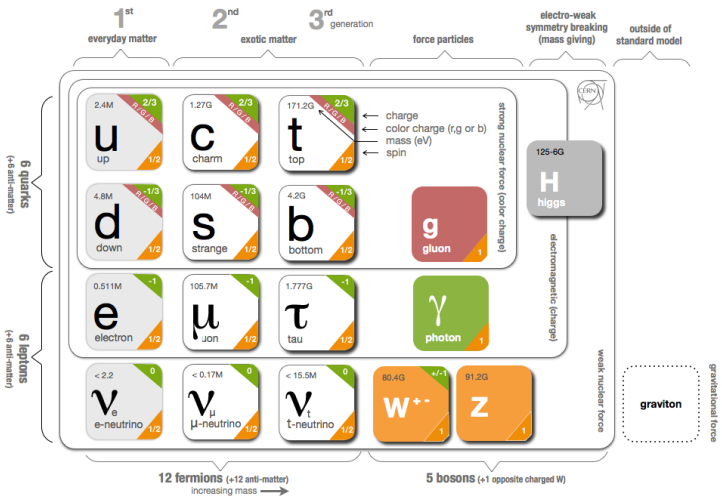

FIGURE 2.1: Fundamental particles of the Standard Model. From (*Purcell, 2012*) [11].

According to the SM, the constituents of matter, *fermions*, can be classify into two groups of particles named *leptons* and *quarks*, all of them with spin of $1/2$. Fermions are also subdivided into 3 generations according to their mass hierarchy, as shown in Figure 2.1. In contrast to leptons, quarks are color-charged and they interact via the strong interaction combining together to form hadrons [12]. Additionally, fermions have a counterpart called *antifermions* with the exact same mass but opposite charge.

On the other hand, the mediators responsible for the interactions are called *bosons* and are divided into gauge or vector bosons (spin 1) and a scalar boson (spin 0). Gauge bosons are summarized as follows: Photon, the carrier of the electromagnetic force, three massive bosons $W^{\pm}$ and Z, the carriers of the weak force, and finally, eight massless gluons responsible for the strong force [13]. The special case of the mass acquired by the $W^{\pm}$ and Z bosons is explained through the electroweak spontaneous symmetry breaking [14], in which a scalar boson, called *the Higgs Boson*, was predicted by the Higgs mechanism and in 2012 it was announced the discovery of a new particle compatible with the predicted Higgs boson by the CMS and ATLAS experiment [15, 16].

2.1.1 Hierarchy Problem

The SM is expected to be a valid theory to energy scales up to $\Lambda^2 \approx M_P^2$, being the Planck mass approximately $M_P \sim 10^{19}$ GeV; the scale of energy in which gravity effects are a deal. Thus, as the Higgs mass obtained is way smaller than the one expected for a scalar boson, huge quantum corrections above the electroweak (EW) scale are required for the SM to be treated as an effective field theory,

$$\Delta m_H = m_H - m_H^0 \sim \Lambda^2 \tag{2.1}$$

However, the Higgs boson acquires quadratically divergent values. To keep the Higgs mass at an acceptable value of $\sim$ 100 GeV, it is required a fine tuning of the parameters in the SM at energies above the EW. This is considered *"unnatural"*, since there is no symmetry involving that sort of necessary couplings [17, 18]. This is the

so-called *hierarchy problem*. So far, the most attractive and well-studied solutions are the theory of Supersymmetry (SUSY) [19], theories involving extra dimensions and the *Little Higgs* theories [18].

2.1.2 Other Limitations of the SM

The SM has provided answers that have been remarkable in the understanding of nature, but there are still open questions that need to be solved, in order to seek for what is yet to be discovered. In principle, there a set of questions that imposes limitations on the SM: the structure of the SM itself, the relation of particle physics and the large scale Universe and questions about the nature of space and time [12]; which are currently matter of study at CERN LHC. A few open questions are:

- Why does the Universe contain more matter than antimatter? This is know as the *Baryon asymmetry.* It seems like the universe requires new *CP*-violating interactions not yet observed.
- What is dark matter? Most of the matter in the universe is *dark matter*, presumably made of particles, which are not accounted by the SM. In particular, possible candidates for dark matter particles emerge naturally from theories of supersymmetry (SUSY) such as R-parity conserving SUSY.
- Are there symmetries of space-time that lead to new particles and interactions?
- How does gravity fit in the scenario of particle physics?

2.2 Extensions of the SM with Long-Lived Particles

The nature of the Hierarchy Problem singles out the electroweak scale for new physics searches, where possible solutions lie in new massive particles. In particular, Long-Lived Particles (LLP) arises from predictions in many theories of physics beyond the Standard Model (BSM), where the macroscopic decay lengths of such particles emerge naturally from the breaking of symmetries. Bearing that in mind, it becomes important to recall the expression for the proper lifetime τ of any particle,

$$\tau^{-1} \sim \frac{1}{2m_X} \int d\Pi_f |M(m_x \to \{p_f\})|^2 \tag{2.2}$$

where m_x is the mass of the particle, M the matrix element governing the decay into products $\{p_f\}$, $d\Pi_f$ the Lorentz-Invariant phase space for the decay and Γ the decay width [17]. In order for a particle to be long lived, its decay width must be small or, in other words, its matrix element or phase space must be small. This could happen if the matrix element is suppressed by means of a symmetry that forbids the decay or by a small effective coupling constant. This is rather familiar, as it is known that the proton long lifetime arise for its decay being forbidden by the baryon number (an accidental symmetry of the SM) or, in the case of the muon long lifetime that arises from a small coupling, the Fermi constant G_F, in a large dimensional scale, high mass of the W boson [20].

Some of the models that could present this behavior and that are being considered in LLP searches at LHC are supersymmetric theories or models with and extended Higgs Sector.

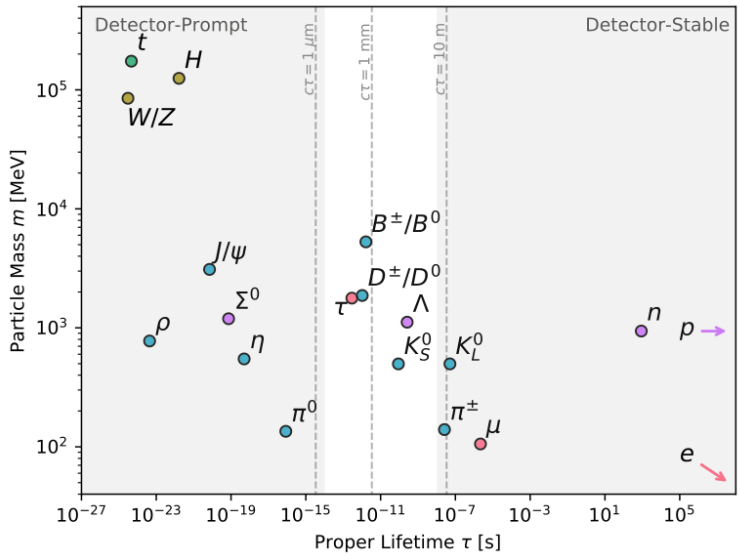

FIGURE 2.2: Standard model particles as a function of mass and proper lifetimes. From *(Lee, 2019)* [17]

2.2.1 Extended Higgs Sector

Models that include extended Higgs sectors have at least three neutral bosons, one of them being the SM Higgs Boson (125 GeV) [21]. Long-Lived Particles (LLP) could couple to the SM-like Higgs boson or to exotic bosons. As for the first kind of coupling, there are possible ways in which LLP are produced through SM-like Higgs bosons, where the dominant production is via gluon fusion and the expectation is to have LLP candidates below of half the mass of the Higgs boson in which the branching fraction into LLP is taken as a free parameter. However, many theories predict new scalar states produced alike SM Higgs and in contrast, the Higgs mass can be taken as a free parameter [22].

Since LLP could arise from hidden sectors, exotic Higgs boson decays are a good possibility for their production mechanism [23]. In particular, a toy model describing the decay of Higgs boson to a pair of pseudo-scalar X bosons that decay back to SM particles ($H \rightarrow XX \rightarrow SM$) [1, 23] is relevant in 2HDM+S [3], NMSSM[4] and in Hidden Valleys models [24].

This motivates the search of LHC LLP and, in particular for the present analysis, it motivates the study of the general signature given by the toy model of non-SM Higgs boson where LLP decay to dileptons (electrons and muons), as shown in Figure 2.3. Here the mass of the Higgs boson is taken as a free parameter[5].

2.2.2 Supersymmetry (SUSY)

Supersymmetry (SUSY) is one of the most well-known theories which try to provide a solution for the hierarchy problem. To achieve that, new symmetries that

[3]Two Higgs Doublet Model with an additional scalar

[4]Next-to-Minimal Supersymmetric Standard Model

[5]In particular for this analysis, the simulation of this process is carried out with $m_H = 400$ GeV. This is further described in Chapter 5

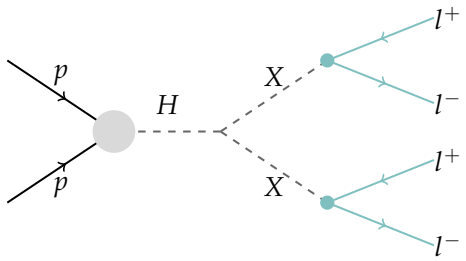

FIGURE 2.3: Production of long-lived spinless bosons X, which subsequently decay to dileptons

allow operations under spin states are added and, as a result, the value of a spin state changes by $1/2$ [23]. In other words, SUSY is a symmetry involving bosonic and fermionic degrees of freedom, meaning that for every SM boson there is a new fermion with the same quantum numbers and for every SM fermion, there is a new boson with the same quantum numbers; such new particles are referred as *supersymmetric partners* [20]. However, supersymmetric particles have not been observed yet, pointing out that, in order for SUSY to hold, the symmetry between fermions and bosons must be broken and their supersymmetric partners should have larger masses (100 GeV- 1 TeV) [25].

The Minimal Supersymmetric Standard Model (MSSM) is the simplest SUSY model that includes the SM which, besides to add the supersymmetric partners to each SM fermions and SM bosons, it also includes 5 supersymmetric partners of the Higgs Boson. In this model, a new symmetry is introduced, called the *R-Parity*, which is conserved and their values for SM particles and SUSY partners are 1 and -1, respectively. Within the MSSM, LLP could arise through a hierarchy of mass scales [22] or as a result of the R-parity symmetry approximation [26] that will be further described in the following subsection.

RPV Supersymmetry

The MSSM let to write renormalizable operators that violate baryon and lepton numbers as it predicts new scalar fields charge under SM gauge interactions. However, such flavor violations are constrained by low-energy experiments and thus, the minimal solution lies in imposing a global symmetry, called *R-parity*, to such renormalizable operators [20]. Under the R-parity symmetry, the lightest supersymmetric particle (LSP) is stable, pair-produced and, in principle, its signature can be detected through MET at LHC. Since searches on LSP have yielded no results, a plausible explanation is that SUSY manifests itself in a non-minimal way, in which R-parity violating interactions could be consider as sufficiently small and therefore, LSP could decay to SM particles via those interactions. As a result, LLP emerge as a feature of RPV operators being highly constrained from flavor measurements, resulting in small RPV couplings [17]. This theory is called *RPV Supersymmetry* and is an extension of the MSSM [20, 26].

Chapter 3

The Experimental Device

The outgrowth of experimental studies of nuclear and cosmic-ray physics have made possible the study of interactions of particles at relatively high energies (up to 100 MeV) and thus to understand their behavior at small distances ($\sim 10^{-15}m$). Nevertheless, the reliability of the observations in cosmic rays were not enough given their uncertain composition and diverse energy and momentum; as a result, particle accelerators were necessary in order to achieve higher trustworthiness and reproducibility as well as higher energy regimes. Thus, modern particle physics began to explore further the basic components of matter and their interactions as particle colliders were becoming more powerful [27, 28].

On the other hand, despite the great success of the Standard Model (SM) to describe phenomena up to energies around TeV provided by high energy colliders, there are still open questions that point out to the existence of physics beyond the Standard Model (BSM). Consequently, improvements on experimental setups such as higher luminosity along with searches for new and exotic particles that could give a hint on a deeper theory, are being carry out. In particular, the Large Hadron Collider (LHC), the most powerful and largest particle accelerator in the world, aims to find experimental explanation to answer such questions [29, 28].

Furthermore, large particle detectors are built around the LHC to analyze a variety of particles produced at the four location points of collisions. One of them, the Compact Muon Solenoid (CMS) allows to depict a wide range of physical phenomena and to measure the properties of discovered particles with high precision. With the purpose of understanding better the experimental setup of the present work, this chapter provides a brief introduction on both the LHC accelerator and the CMS detector.

3.1 The Large Hadron Collider

The Large Hadron Collider is a superconducting synchrotron built by the *European Organization for Nuclear Research* (CERN), located across the Swiss and French borderline near Geneva. The LHC machine is a circular proton-proton (pp) collider as well as a heavy ion collider with a perimeter of 27 km, about 100 m underground [30]. This accelerator complex is formed by 8 sectors (LINAC2 and 3, PSB, PS, SPS,AD,ISOLDE, LEIR) interconnected through 4 straight regions of 540 m, where the detectors are located: ALICE [1], CMS [2], LHCb [3] and ATLAS [4]. A schematic view of the LHC is shown in Figure 3.1.

[1] A Large Ion Collider (ALICE) [31]
[2] Compact Muon Solenoid (CMS) [32]
[3] Large Hadron Collider Beauty (LHCb)[33]
[4] A Toroidal LHC ApparatuS (ATLAS) [34]

At the beginning of the accelerator chain, protons are obtained from the injection of Hydrogen gas into the metal cylinder, known as Duoplasmatron, surrounding it with an electric field to break down the gas into its constituents. Afterwards, protons are sent to the linear accelerator (LINAC2) where they are accelerated up to 50 MeV and heavy ions are sent to LEIR. Soon, protons reach energies of up to 1.4 GeV at the circular accelerator known as Proton Synchrotron Booster (PSB) and in few microseconds they are injected into and accelerated in the Proton Synchroton (PS) and Super Proton Synchrotron (SPS) to 25 GeV and 450 GeV, respectively. Finally, protons are transferred to the LHC Ring, both in a clockwise and counterclockwise direction, reaching energies of 13TeV after 12 *"supercycles"* [29, 30].

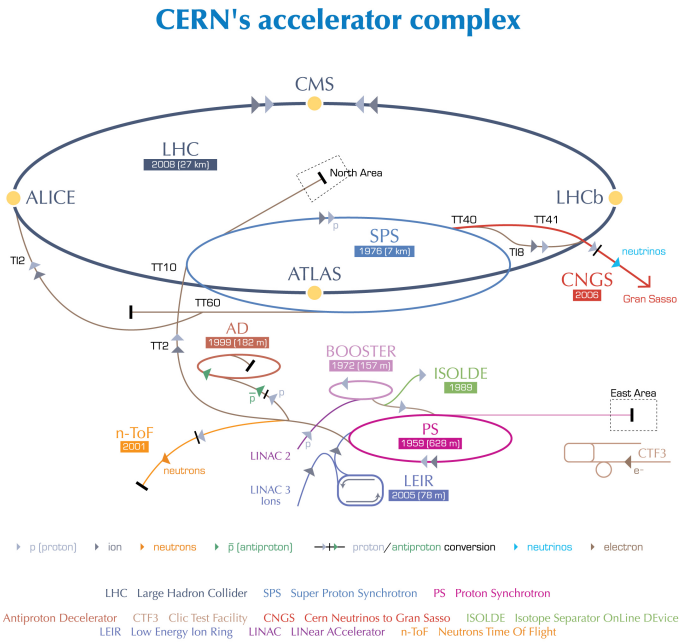

FIGURE 3.1: The CERN accelerator complex. From (*Lefèvre, 2008*) [35].

3.2 The CMS Experiment

The Compact Muon Solenoid (CMS) is a general-purpose detector which central feature is a superconducting solenoid, with an internal diameter of 5.9 m that provides an axial field of 3.8 T. Within the field volume are the silicon pixel and strip tracker, a fully active scintillating crystals-based electromagnetic Calorimeter (ECAL) and a Hadronic Calorimeter (HCAL); making CMS a relatively compact detector [1]. With all that, the CMS has been design to make measurements in a wide range of high energy physics spectra: from Standard Model properties to search of exotic processes. A schematic view of the CMS experiment can be found in Figure 3.2.

The main goals of CMS are to explore and address physics at the TeV scale and to be prepared for searching of new particles. To achieve that, the detector requirements are summarized as follows [36]:

- Good muon identification and momentum resolution, $\sim$ 1% di-muon mass resolution at $\sim$ $100 GeV/c^2$ and the ability to determine unambiguously the charge of muons with momentum up to $1 TeV/c$.
- Good charge particle momentum resolution, di-photon and di-electron mass resolution, hermeticity and efficient photon and lepton isolation at high luminosities.
- Good MET and di-jet mass resolution requiring hadron calorimeters with large hermetic coverage and fine lateral segmentation.

The four CMS subdetectors: The silicon tracker (3.2.2), the ECAL (3.2.3), the HCAL and the Muon System (3.2.4) will be described in the following subsections of this chapter, together with the trigger and datasets (3.2.1) necessary to select events of interest.

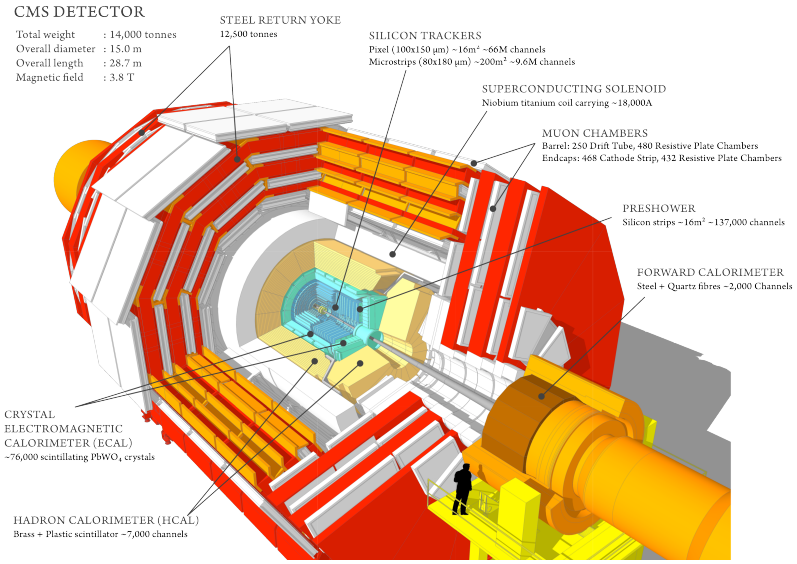

FIGURE 3.2: Sectional View of the CMS detector. From (*Sakuma,et.al, 2014*) [37].

3.2.1 Trigger, Datasets and Simulated Samples

The LHC has an event rate of $\sim 1 GHz$, about one billion proton-proton interactions per second, making data acquisition and storage capacity a challenge. To overcome this, a trigger system able to select potentially interesting events and reduce the acquisition rate was implemented and currently employed for each of the different experiments at CERN [38]. In particular, the rate acquirable by the CMS experiment is around $1 kHz$, where its trigger system is divided in two levels: Level-1 (L1) trigger and the High Level Trigger (HLT). The first one, based in hardware on the calorimeter and muon system, provides an output rate of $100 kHz$. On the other hand, the HLT relies on software designed to reconstruct the *particle flow* from complex *"link"* algorithms able to synchronize information from each sub-detector and

[1] see Chapter 4 for a more detailed discussion.

to reject uninteresting events [39, 40]. This last trigger reduces the ratio to about $1kHz$ and contributes to achieve a good resolution and online event reconstruction for the experiment [41].

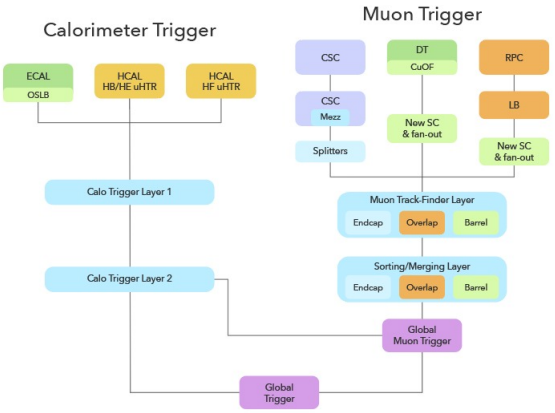

(A) L1 Trigger architecture

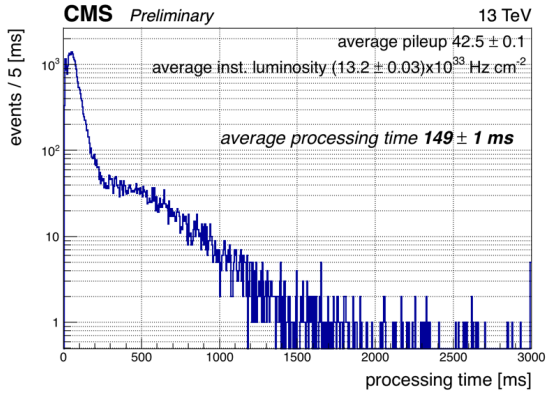

(B) HLT processing time (*Set,2019*) [40]

FIGURE 3.3: Scheme of Level-1 Trigger and the HLT processing time

Furthermore, datasets are defined according to the particle flow reconstruction given by the High Level Trigger. Specifically, the primary datasets are defined by a set HLT paths that target different physics processes and thus, collect events with similar physics content [42]. In the present analysis, events were collected by the CMS detector at the LHC during Run II at a centre-of-mass energy of 13TeV, and selected from data samples corresponding to 35.87 fb^{-1} of integrated luminosity.

Simulated samples are used in this analysis for signal and the main 2 background processes: $Drell - Yan$ and $ttbar$ pair production. For signals `PYTHIA v8` [43] is used to simulate H production through gluon-gluon fusion.

The tt events are generated using `POWHEG(v2)` [44], while $Drell - Yan$ production is simulated using `MADGRAPH5aMC@NLO` [45]. In both cases, `PYTHIA v8` is used for the parton shower. After this generation step, the simulation of the response of the CMS detector is carried out with `GEANT4` [46].

3.2.2 The CMS Tracker

The measurement of momenta and tracking detection of charged particles is a fundamental aspect of high energy physics experiments. While the measurement of energy is mostly provided by calorimeters (see Subsection 3.2.3), the momenta are measured by precise tracking systems in a magnetic field: By detecting the ionisation of charged particles, it is possible to reconstruct the *"trail"* of ionised atoms and measure the curvature of the particles' trajectory along the magnetic field (see Figure 3.4). Moreover, high precision vertex detectors are positioned near the interaction point, allowing to recognized secondary decay vertices which are displaced from the collision [47].

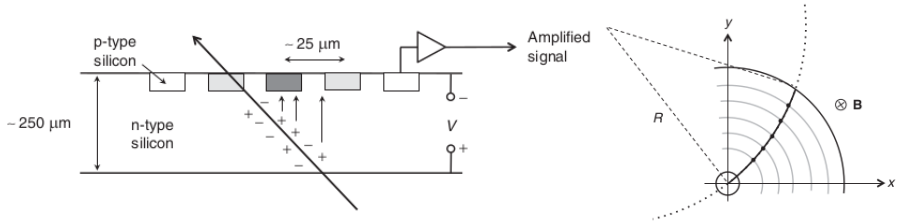

(A) Schematic view of a traversing particle in a silicon detector.

(B) Track reconstruction in a silicon detector.

FIGURE 3.4: Traversing particle in silicon detectors. From (*Thomson,2019*) [48]

Accordingly, the purpose ot the CMS tracker detector is to reconstruct the primary and secondary vertices of an *event*, as well as to measure the momenta of charged particles. The tracking detector is located in the innermost region of the CMS experiment (see Figure 3.2) and it is arranged in multiple silicon layers capable of measuring the position of a traversing particle [49]. Due to the high track density achieved by its proximity to the interaction point, the current CMS tracker is entirely composed by silicon micro-strip and pixel detectors, providing a high position-sensitivity resolution. In addition, there are many advantages by using silicon detectors in the CMS tracker, such as: Excellent detection capabilities (*e.g.* high efficiency and fast charge collection) and the availability of developed technology for complex and granular sensors [47].

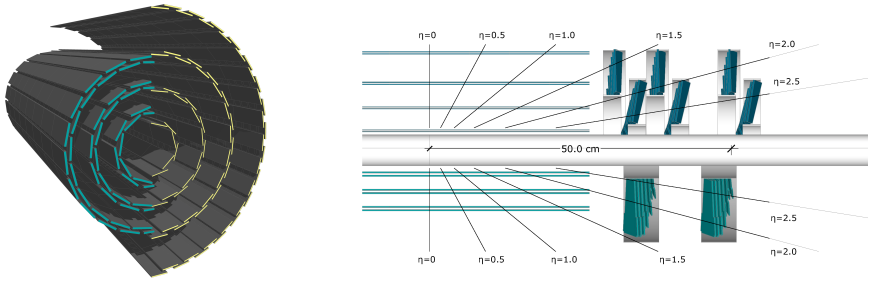

(A) The pixel Tracker.

(B) Geometry of the Tracker

FIGURE 3.5: The Silicon Pixel Detector (SPD). From (*Sakuma,et.al, 2014*)[37]

[1] a collision between two protons.

Furthermore, the CMS tracker system consists of a cylindrical volume of $5.8m$ in length and $2.5m$ in diameter, with its axis aligned to the LHC beamline. On the one hand, the Silicon Pixel Detector (SPD) located in the inner part of the tracker is compressed in three barrel layers and four end-cap disks. It has around 1000 silicon sensor modules segmented into 66 million $(150 \times 100)\mu m^2$ pixels which provides three-dimensional position measurements of the hits arising from their interaction with charged particles [50]. In total, the SPD covers the region of $|\eta| \leq 2.6$ and basically, it is used to reconstruct secondary vertices. On the other hand, the Silicon Strip Detector (SSD) surrounds the three barrel layers of the SPD with ten layers of micro-strip detectors. It has approximately 15000 silicon sensor modules finely segmented into 9.6 million 80-to-180 μm wide strips [49].

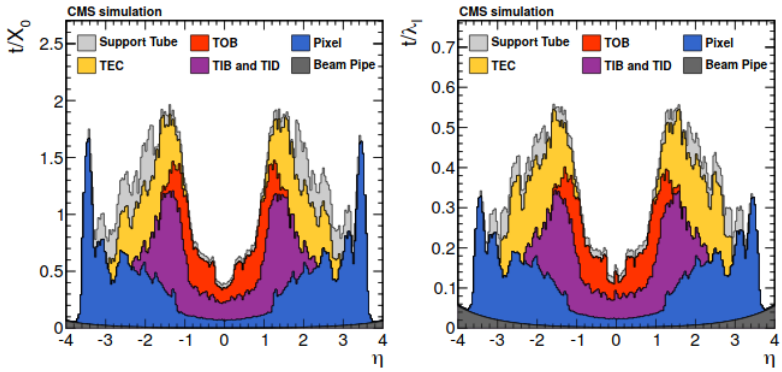

FIGURE 3.6: CMS Tracker material budget. Total thickness t of the tracker material as function of pseudo-rapidity η, expressed in units of radiation length X_0 (left) and nuclear interaction length λ_I (right). From (*The CMS Collaboration, 2014*) [49].

The SSD consists of 4 subsystems: The Tracker Inner Barrel (TIB), the Tracker Inner Disks (TID), the Tracker Outer Barrel (TOB) and the Tracker EndCaps (TEC). The first two, the TIB and TID, provide position measurements in the $r\phi$-plane with a resolution of $\sim 13 - 38\ \mu m$. The TOB provides a resolution of $18 - 47\ \mu m$ within $r > 55cm$ and $|z| < 118cm$ in the $r\phi$-plane. And lastly, the TEC covers a region of $(124 < |z| < 282)cm$ [49]. To summarize, the spatial resolutions achieved by the CMS tracker are shown in Table 3.1.

Subsystems	*CMS Tracker Detector*			
	Location		Resolution ($r\phi$)	Resolution (z)
SPD (barrel)	$4.4 < r < 10.2\ cm$	–	$15\ \mu m$	11-17 μm
SPD (endcap)	$34.5 < \|z\| < 46.5\ cm$	–	$15\ \mu m$	$90\ \mu m$
SSD (TIB)	$20 < r < 55\ cm$	–	$13\ \mu m$	$38\ \mu m$
SSD (TID)	$58 < \|z\| < 124\ cm$	–	$15\ \mu m$	μm
SSD (TOB)	$55 < r < 116\ cm$	–	$18\ \mu m$	$47\ \mu m$
SSD (TEC)	$124 < \|z\| < 282\ cm$	–	$\sim 18\ \mu m$	$\sim 47\ \mu m$

TABLE 3.1: A summary of location and resolution of the subsystems in the CMS tracker detector.

As shown in Figure 3.6, the layers of SPD and SSD have considerable amount of material in front of the calorimeters. For instance, the material budget [1] reaches 180% of radiation length at $\eta = 1.5$, mostly due to TEC. This represents a limitation to the resolution of the electromagnetic calorimeter, since particles are loosing energy in the layers before reaching the calorimeters [50, 51].

3.2.3 The Electromagnetic Calorimeter (ECAL)

As charged particles leave hits in the tracker and muon systems (see Subsections 3.2.2 and 3.2.4), the electrical signal produced by their passing through calorimeters can be interpreted as energy deposits. In that sense, the CMS experiment is equipped with an electromagnetic calorimeter (ECAL) made of lead tungstate ($PbWO_4$) crystals and photodetectors specially designed to operate within the high magnetic field (3.8 T). This allows to precisely measure the energy of electrons and photons together with a fraction of the energy of jets coming from electromagnetic showers [39, 52].

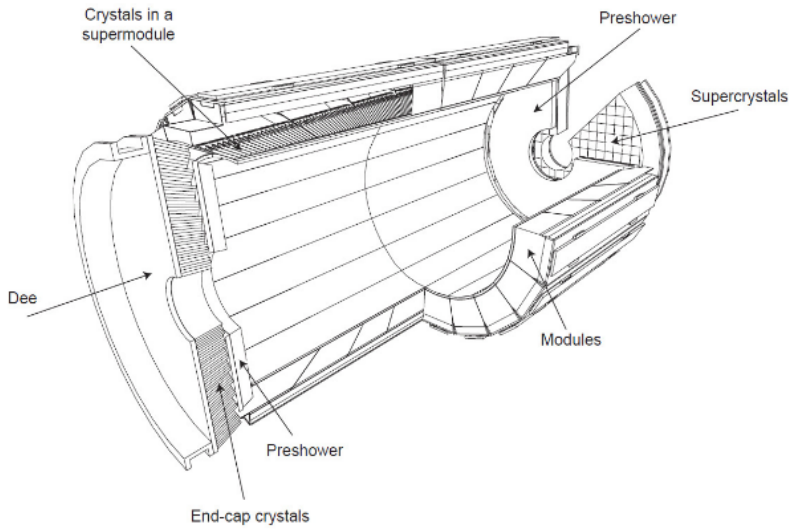

FIGURE 3.7: Layout of the CMS ECAL, showing the barrel, the two endcaps and the preshower detectors.From (*Chatrchyan et.al, 2010*) [53].

The ECAL, composed of a barrel section and two endcaps, is located between the tracker detector and the HCAL[1]. The barrel covers a region of ($|\eta| < 1.479$) and consists of 61200 crystals formed into two rings of 18 so called *"supermodules"*[2] [54]. On the other hand, each endcap is made of 7324 crystals and, together covers a pseudo-rapidity range of ($1.479 < |\eta| < 3$). In addition, pre-shower detectors composed of silicon micro-strips are added in front of each endcap; covering a range of ($1.65 < |\eta| < 2.6$) [54, 55]. The structure of the ECAL is shown in Figure 3.7.

[1] In other words, the detection efficiency in the tracker fiducial volume

[1] Hadronic Calorimeter

[2] 1700 crystals comprised of $\sim 26X_0$.

3.2.4 The Muon System

The CMS experiment was designed to be a powerful muon spectrometer and thus, one of its most important tasks is the precise measurement and detection of muons. In order to efficiently trigger and identify them, the CMS muon system is composed of three layers of steel interleave with four detectors, as shown in Figure 3.8. The detectors are based in three different technologies: Drift Tubes (DT) chambers in the barrel, Cathode Strip Chambers (CSC) in the endcaps and, complementing the CSC, the Resistive Plate Chambers (RPC).

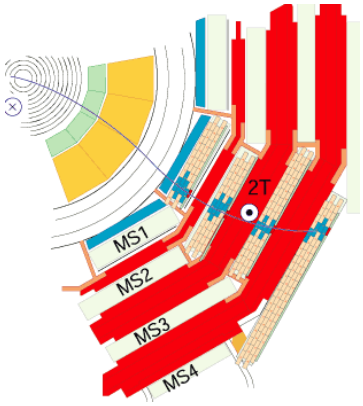

(A) Lateral View.

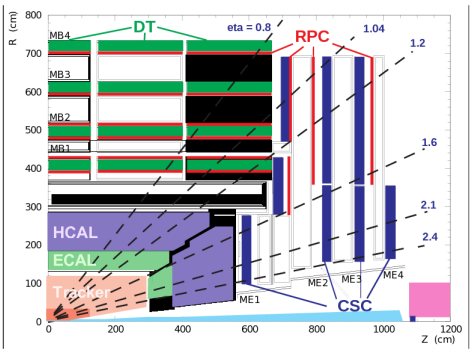

(B) Longitudinal View of one quadrant of the CMS.

FIGURE 3.8: Schematic view of the CMS muon system. On the left, the lateral view shows the trajectory of a muon. On the right, the DT stations in the barrel (green), the CSC stations in the endcap (blue) and the RPC stations (red) are presented.From (*Paolucci, 2005*)[56]

The pseudo-rapidity regions cover by the DT chambers and CSC are ($|\eta| < 1.2$) and ($0.9 < |\eta| < 2.4$) respectively, while RPC covers the range ($|\eta| < 1.6$) [39]. On the other hand, the reconstruction involves both the muon detectors and the inner tracker and therefore, it improves the resolution for muon transverse momentum from $8\% - 15\%$ at $10GeV$ to $1\% - 1.5\%$ at $10GeV$, and from $20\% - 40\%$ at $1TeV$ to $6\% - 17\%$ at $1TeV$ [52].

Chapter 4

Event Reconstruction at CMS

The *pp* collisions at LHC produce a large amount of signatures that leave an electrical signal in each CMS detector, as described in Chapter 3. Thus, the proper identification and reconstruction of high-level physics objects[2] is carried out by advanced algorithms, which are specifically designed to take the raw pieces of information provided by the signals. This information is associated together to determine points (*i.e* hits) in the particle trajectory and therefore, used to determine the type of particle and its properties: momentum, charge and energy. In particular, the particle flow (PF) algorithm deployed in the CMS experiment allows high performance for the reconstruction of MET and jets as well as for the identification of muons and electrons, by coherently combining information for the different subdetectors [57, 39].

In this chapter, a general description is given for the reconstruction of specific PF elements used in the present analysis: muons and electrons along with primary and secondary vertices reconstruction.

4.1 Muon Reconstruction

Muons are well known for being fundamental charged particles and for having relatively small energy loss in matter, in contrast with other charged particles. As a result, they easily pass through the CMS detector before decaying, allowing them to be tagged as stable by the reconstruction algorithms. Additionally, the muon signature is identified by quantifying the compatibility between reconstructed tracks in the inner tracking system and the hit information in the muon detectors along with small energy deposits in the calorimeters [58, 59]. As such, identification and reconstruction algorithms are designed to identify muons with high efficiency and low probability of misidentification, together with a good specification of their passage through detectors.

This section gives an overview of the different algorithms to reconstruct a muon as a PF candidate. Essentially, there are two main algorithms depending on the information used,

- **Standalone Muons** (SM): Based on information from the muon system.
- **Global Muons** (GM): Based on hits in the muon system and the silicon tracker.

The interest f the present analysis relies upon these two algorithms (SM and GM), including the displaced counterparts introduced in Run 2 (displaced SM and displaced GM); the following subsections will focus on the previously mentioned algorithms.

[2] such as the particle-flow algorithm (PF)

Standalone Muon Reconstruction

The standalone algorithm is built by exploiting information from the different subdetectors in the muon system.Those that present an electric response participate in the offline reconstruction in which track segments are built using a linear fit.

As an initial estimation, these segments are used to generate seeds consisting of position, momentum and direction vectors for the Kalman-Filter technique[1]. Subsequently, the fit performed is propagated to the next chamber (known as *prediction*) in order to search for a compatible segment, called *measurement*, to properly reconstruct the trajectory of the muon [59, 61]. In essence, standalone muons come from the information gathered in the CSC, DT and RPC subdetectors (see Chapter 3) allowing the reconstruction of a muon trajectory using a Kalman-Filter technique [62].

Global Muon Reconstruction

The global muon algorithm extends the muon trajectories in the muon system by including hits in the silicon tracker. The reconstruction starts from a standalone muon track, where the muon trajectory is extrapolated from the innermost chamber to the outer tracker system, looking for a match between standalone muon and tracker tracks[2] [63, 61]. The compatibility of both tracks is based on the extrapolated trajectory's parameters and their corresponding uncertainties, with the assumption that the muon originates from the interaction point. Once the best matching is selected, a combined fit using all hits in both tracks is performed with the Kalman-Filter procedure and as a result a collection of tracks referred as *Global Muons* is obtained [61].

The momentum resolution for a muon track of $p_T \leq 200 GeV/c$ is driven by measurements in the silicon tracker (tracker muons). Nevertheless, as momentum increases and the curvature of its track decreases, momentum resolution becomes limited and approaches as the *global muon reconstruction* improves the p_T measurement by fully exploiting the information from both tracker and muon detectors [63].

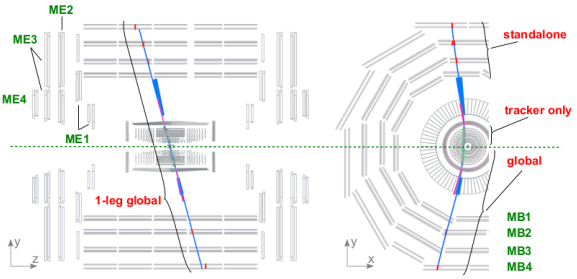

FIGURE 4.1: Schematic view of a cosmic muon crossing CMS: .From (*CMS collaboration, 2010*) [63].

Displaced Standalone Muon (DSM) Reconstruction

In contrast to the standard standalone reconstruction, the new algorithm for Run 2 is designed for muons produced in decays far away from the interaction point as well as for decays with a significant delay with respect to the time of collision. Similar to the standard algorithm, segments in the muon chambers are seeded by groups

[1] see *Track Reconstruction in the CMS Tracker, page 143-147, T.Speer,et.al*[60]

[2] Tracks reconstructed in the tracker system

and for each seed, a muon track is reconstructed using the Kalman-Filter Technique with the difference that there is no constraint to the interaction point. In addition, the DSM exploits information from a new algorithm for segment reconstruction in the barrel Drift Tube (DT) chambers, allowing a better performance for out-of-time particles[3]. It has also been implemented for the HLT, bringing a significant improvement to the trigger efficiency for both displaced and delayed muons [64].

Displaced Global Muon (DGM) Reconstruction

The new implementation for global muons is designed for displaced-in-time muons produced within the inner tracker volume, where hits leaved by a muon in both inner tracker and muon chambers are taken into account. The new global muons arise as a way to optimize the reconstruction for displaced muons with the help of a specific *displaced-muon tracking (DMT)* implemented in the inner tracker [64]. Basically, the displaced-muon tracking is seeded by the DSM and, as previously mentioned, it does not use constraints to the interaction point in the pattern recognition nor the track fit. Finally, as the best match between DSM and DMT is found, the fit is performed and the displaced global muons are obtained.

For this study, the thresholds for the two tracks of muons candidates must satisfy $p_T > 25$ GeV/c and, also, must be oppositely charged [1]. Additionally, the reconstruction chosen for muons was DGM since the LLP of interest are assumed to decay in the tracker and thus, their decay length ($c\tau$) should be below than ~ 600 cm [1, 22]; in contrast to DSM that allows to reconstruct muons that decay beyond the tracker detector and therefore, LLP with longer lifetime could be explored. Nonetheless, the prior reconstruction used in Run 1 was based on identifying muons as tracks that can be matched to *trigger objects* (SA muons) from a given HLT path within a cone of size $\Delta R < 0.1$ and disregarding any PV constraint, where both tracks and SA muons are extrapolated to the beamline [59]. One motivation of the present study is to compare the performance between both muon reconstructions: Muon Run1-like and DGM Run2-like algorithms.

4.2 Electron Reconstruction

Electrons, known for being charged and electromagnetic particles, interact with the tracker system and the electromagnetic calorimeter (ECAL) in the CMS experiment. As electrons propagate through the tracker layers, they lose energy due to bremsstrahlung and start to emit photons before they reach the ECAL. Thus, by the time electrons reach the calorimeter, an electromagnetic shower is produced and most of its energy is deposited and clustered together by a small number of crystals. Hence, to reconstruct the energy of the primary electron it becomes necessary to recognize and combine each energy deposit[4] from the bremsstrahlung photons produced by the electron. In summary, the first stage for the electron reconstruction consists of combining clusters from the ECAL and thus to measure the electron energy, known as superclustering [65, 25]. Since the electron signature also involves hits in the inner tracker, the next step is the tracking algorithm. Then, a match between both the track and the energy is carried out to finally be combined as the full electron trajectory [52].

[3] see Performance of the Mean-Timer Algorithm

[4] Also known as cluster

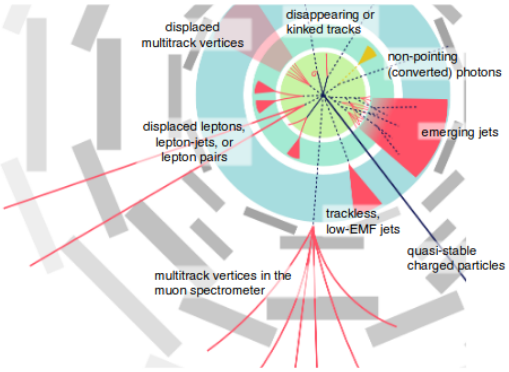

FIGURE 4.2: Schematic of atypical signatures arising from BSM LLP in the detectors at LHC. From (*Alimena et.al, 2019*) [22].

Supercluster Reconstruction

The signals due to electrons or photons in the ECAL are stored in small crystals (See Chapter 3.2.3) and the energy deposit is usually spread out over several crystals in the ϕ coordinate, when photons and electrons are irradiated via bremsstrahlung. Therefore, clusters are gathered together,starting from the crystal with an energy deposit above a certain energy threshold (seed) and adding the corresponding energy in adjacent crystals. As a result, a group of crystals around the seed is obtained and called *Supercluster* (SC). The SC energy corresponds to the sum of energies of all its clusters and it is essential for measuring accurately the initial energy of the electron [52, 65, 25].

Electron Track and GSF Reconstruction

Despite the fact that electron tracks can be reconstructed using the Kalman-Filter Technique used for muon reconstruction, a dedicated tracking algorithm is used for electrons because of their radiative losses in the tracker material. As the SC is obtained, its position and energy are used to extrapolate the electron trajectory towards the nominal vertex in order to find compatible hits in the tracker. Once the tracker seeds are set up, they are then fitted using a Gaussian Sum Filter (GSF). The final reconstruction is the merging of the SC and track information [65, 66, 25].

4.2.1 Electron Reconstruction for Displaced Vertices

As previously discussed (see Chapter 3.2.1), the LL particles candidates here considered decay to a pair of charged-leptons. With the purpose to improve the efficiency for reconstructing leptons from displaced vertices, the selection criteria for the electron channel are slightly tuned and they are separated into *photon candidate* and *electron candidate*.

Photon Candidate

Photon candidates are identified as ECAL energy clusters that are not linked to other charged particles' trajectory in the calorimeter. Photons considered in this analysis are required to satisfy for the leading(subleading) photons: $p_T > 30(20)$ GeV/c and $|\eta| < 2.5$ [67]. Once an energy deposit in the ECAL is reconstructed as a photon,

the match with a track within a cone of size $\Delta R < 0.1$ is performed, in order to be identified as originating from an electron [1].

Electron Candidate

The thresholds for electron candidates are slightly more stringent than the trigger requirements, in order to ensure a high trigger efficiency. The selection criteria for the leading(subleading) electron must satisfy $E_T > 40(25)$ GeV and the two tracks associated to the higher(lower) E_T electron must also satisfy $p_T > 41(28)$ GeV/c. The latter allows to suppress electrons that emit large amounts of bremsstrahlung [1].

4.3 Vertex Reconstruction

The reconstruction of vertices of charged particles in the CMS experiment relies on the tracker detector and can be decomposed in two parts: *vertex finding* and *vertex fitting*. The first one consists in a pattern recognition problem, which the main purpose is to disentangle vertices in difficult topologies (*i.e.* from decay near the interaction point) [68]. The latter, vertex fitting, is a statistical problem that aims to compute the location of an interaction vertex from a given set of reconstructed track through the Kalman-Filter technique [68, 69]. In this section, the primary and secondary vertex candidates are briefly described with special emphasis on criteria required for selecting leptons tracks from a LL candidate.

4.3.1 The Primary Vertex

The pp collisions are selected when events contain a primary vertex with no more than 2 cm displaced from the nominal interaction point transverse to the beamline and no more than 24 cm in the direction along the beam. Additionally, the primary vertex is required to be associated to at least 4 tracks [1]. Essentially, primary vertex candidates are obtained by clustering preselected tracks based along the beamline, where their impact parameter significance and p_T are taken into account. Afterwards, a vertex fit is performed to estimate the vertex position using sample of tracks compatible with being originated in the interaction region. The primary vertex selected is the one with the highest sum over p_T^2 of associated tracks [70, 69].

4.3.2 The Secondary Vertex

Secondary vertex candidates are set after selections on the primary vertex and upper cuts on the invariant mass, using a robust fitter called *"Trimmed Kalman Vertex Fitter"*[5] (TKF). The secondary vertices are fundamental to identify heavy flavor decays and have been used as well in b-tagging algorithms [70, 72]. For highly displaced vertices, the lepton identification requirements are less stringent than the standard CMS algorithm, in order to maximize the efficiency of reconstruction. The pseudorapidity region is imposed to be $|\eta| < 2$, since tracks from displaced vertices decreases at large $|\eta|$ [1].

[5] see *Section 2.5,T.Speer*[71].

Chapter 5

Analysis

The present study is based on an ongoing analysis of searches for long-lived particles that decay into final states containing displaced leptons in the Run 2 of the LHC, using 2016 data collected with the CMS detector in proton-proton collisions at $\sqrt{s} = 13$ TeV. In particular, this study focuses on the generated samples produced with `PYTHIA v8`, which benchmark model is BSM $H \rightarrow XX \rightarrow 4l$ ($4\mu/2\mu 2e/4e$), where the generated non SM-Higgs boson mass was chosen to be $m_H = 400$ GeV, the scalar X boson mass was set up to be $m_X = 50, 150$ GeV with mean proper lifetimes times τ, such as $c\tau = 4, 40, 400$ mm.

The main purpose of the given analysis is to estimates signal sensitivity from information of generated long-lived particles for a given $c\tau$, in a way that could help to optimize cuts at analysis level. For doing so, it becomes necessary to know how efficient lepton and displaced lepton reconstructions are for the different samples and to choose which signal provides the best trade off between efficiency reconstruction and background rejection. Additionally, this study aims to compare the performance for two different reconstruction algorithms for muons: the Muon Run1-like and DGM Run 2-like algorithms.

This chapter is dedicated to discuss the results obtained: Section 5.1 covers the description of the signal of study, lepton candidates and secondary vertex reconstruction efficiencies (Subsections 5.1.1, 5.1.2) and the overall efficiencies to compare different reconstruction algorithms are shown in Subsection 5.1.3. Secondly, Section 5.2 gives an illustration of the signal sensitivity and optimization of cuts applied; and finally, Section 5.3 offers a way to extrapolate previous results to estimate signals for other values of $c\tau$, where there is accessibility to the events generation but lack of CMS reconstruction for such values of $c\tau$. Also, in Subsection 5.3.1 a brief comment on some aspects that could be matter of further studies is given.

5.1 Standard Event Reconstruction Efficiency and Misidentification

As mentioned before, this analysis is based on MC simulations of BSM $H \rightarrow XX$ signal model and the samples are listed in Table 5.1, where they were produced for a given BSM Higgs boson mass m_H, two combinations of LLP masses (m_X) and different mean proper lifetimes. For the sake of simplicity, the final state here considered is the one in which one long-lived particle decays to two muons and the other to two electrons ($2\mu 2e$). The main backgrounds taken into account are: QCD yielding to dileptons, Drell-Yan yielding to dileptons, W+Jets, Diboson processes and TTJets,

as shown in Figure 5.1. In addition, Table 5.2 summarizes the selection requirements along with the dedicated triggers to collect data containing long-lived particles.

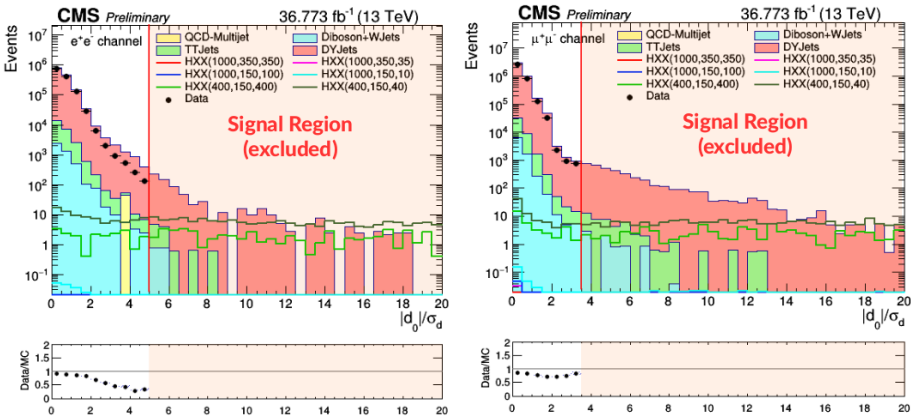

FIGURE 5.1: Data and Monte Carlo comparison in Signal region for e^+e^- channel (left) and $\mu^+\mu^-$ channel (right). From *(CFMadrazo, et.al, 2019)* [73]

Such backgrounds for MC simulation were selected as this study deals with displaced leptons and all Standard Model processes present promptly signatures. Therefore, the main background is instrumental. Additionally, the control and signal region are defined for $|\Delta\Phi| > \pi/2$ and $|\Delta\Phi| < \pi/2$, respectively and being $|\Delta\Phi|$ the collinearity angle in the transverse plane between the dilepton p_T vector and the transverse decay length L_{xy}.

Samples	*Parameters*		
	$m_H(\text{GeV}/c^2)$	$m_X(\text{GeV}/c^2)$	$c\tau$ (mm)
`Sample 1, 2, 3`	400	50	$4, 40, 400$
`Sample 4`	400	150	400

TABLE 5.1: Simulated Signal Samples $H \to XX$ used in the present analysis

The LLP candidate is, thus, selected per event when baseline selection to dilepton candidates are fulfilled, as described in Table 5.2, where it is considered the maximum $|d_0|/\sigma_d$ for the pair of leptons. Lepton tracks are required to have an impact parameter significance $|d_0|/\sigma_d > 5(3.5)$ for electrons(muons), with respect of the primary vertex. This provides a good background rejection together with a high efficiency for the different signals, as shown in Figure 5.1.

Moreover, it is important to highlight what the generated level and reconstruction information are together with their main differences, as it will be mentioned along the analysis. Events generation is the first step to simulate MC samples, which aim is to give a description of outgoing particles produced in a hadron collision by means of general-purpose generators such as `Pythia v8`. After simulating the hard process, the detector electronic responses due to a particle passing through is reproduced and further reconstructed, so as to generate samples comparable to data. The latter demands more computing resources and time.

5.1.1 Lepton Reconstruction Efficiencies

The motivation to study lepton reconstruction efficiencies is to understand how well lepton candidates are being selected for different LLP lifetimes (such that the mean transverse decay lengths $c\tau$ are as shown in Table 5.1), including two different kinematics for the LLP ($m_X = 50, 150$ GeV). Also, a first approach to compare the reconstruction efficiency between Muons-Run1($MR1$) and Displaced Global Muons (DGM) as function of p_T, η, L_{xy} is illustrated.

Channel	*Baseline Selection Requirements*		
	Min. Isotrack p_T(GeV/c)	Min. Superclu-ster E_T(GeV)	Max. $\lvert\eta\rvert$
Electron (e^+e^-)	41, 28	45, 25	1.442
Muon ($\mu^+\mu^-$)	45, 25	–	2.0
HLT paths	`HLT_L2DoubleMu28_NoVertex_2Cha_Angle2p5_Mass10`		
	`HLT_Photon42_R9Id85_ORCaloId24b40e_Iso50T80L_Photon25AND_HE10_R9Id65_Eta2_Mass15`		

TABLE 5.2: Baseline selection requirements and HLT paths of the ongoing analysis of search for LLP decaying to dileptons.

Although this analysis is based on the baseline selection described in Table 5.2, stringent requirements for this study of efficiencies require leptons at a generator level to fulfill the following criteria, in order to achieve flatter efficiencies with respect to the lepton p_T:

- Both generated electron(muon) $p_T > 40(40)$ GeV; *Acceptance Criteria* (5.1)
- Both generated electron(muon) $|\eta| < 1.442(2.0)$;
- Generated X boson $L_{xy} < 20.2226(60.0)$ cm when decaying to electrons(muons).

In addition, for the baseline selection of the present analysis the p_T requirement for reconstruction information was imposed to be 40 GeV for both reconstructed leptons. The fraction of dileptons at a generator level coming from a long-lived X that fulfilled the criteria in (5.1) is defined as the *acceptance* $\mathcal{A}$. Table 5.3 summarizes the acceptances obtained for chosen leptons when fulfilling the first two and full criteria required.

Channel	*Acceptances*			
	`Sample 1`	`Sample 2`	`Sample 3`	`Sample 4`
Electron (e^+e^-)	0.315(0.315)	0.316(0.232)	0.315(0.040)	0.379(0.196)
Muon ($\mu^+\mu^-$)	0.401(0.401)	0.399(0.388)	0.401(0.134)	0.527(0.443)

TABLE 5.3: Acceptances $\mathcal{A}$ for leptons at generator level that fulfilled cuts of p_T, η (and L_{xy}) for each sample.

As shown for electron channel in Table 5.3, the acceptance $\mathcal{A}$ for samples with the same kinematics (`Sample 1,2,3`) is almost identical when generated leptons are

selected only taking into account the first two requirements of the acceptance criteria and similarly, for muon channel, although the acceptances obtained are higher than for electrons, as the requirement for electrons in η is more stringent than for muons. However, when it is also considered the latter requirement for transverse decay length L_{xy} for both electron and muon channels, leptons from samples with smaller values of $c\tau$ fulfilled easily the criteria for L_{xy} as shown for `Sample 1`, while for `Samples 3,4` acceptances become smaller.

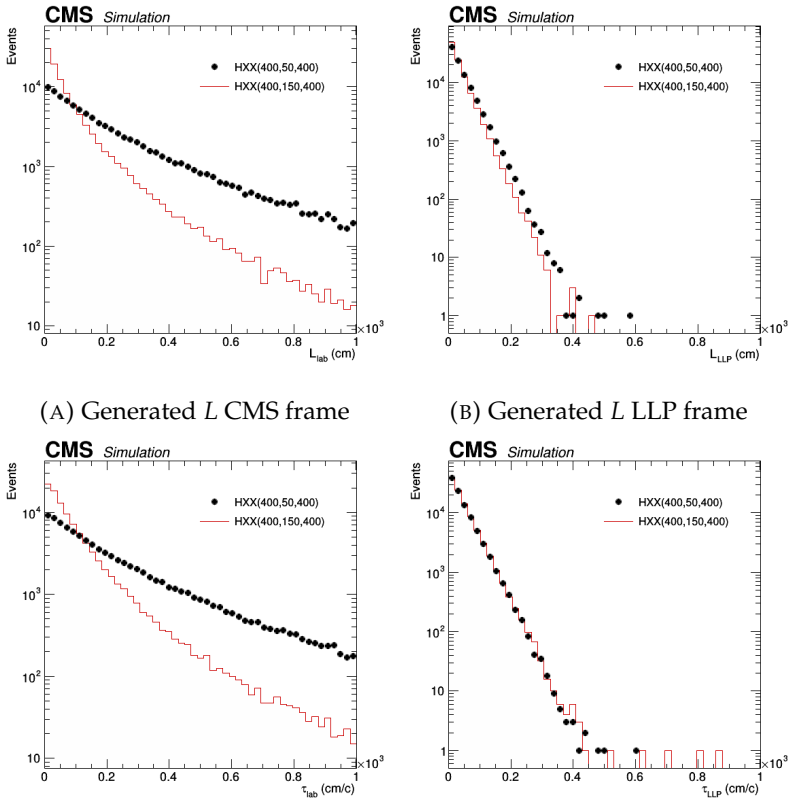

(A) Generated L CMS frame

(B) Generated L LLP frame

(C) Lifetime τ CMS frame

(D) Lifetime τ LLP frame

FIGURE 5.2: Generated L and τ distributions for `Sample 3` (black) and `Sample 4` (red).

Additionally, the fraction of generated leptons after passing criteria in 5.1 for `Sample 3` is significant smaller than for `Sample 4`, even though both samples have the same nominal value of $c\tau$. This is due to the higher mass splitting of `Sample 3` in contrast to `Sample 4`, where to illustrate this better Figure 5.2 shows the lifetime τ and generated decay length L for `Samples 3,4` in two different systems of reference: CMS or lab and LLP frames. As expected, it is found that both samples show a similar distribution when the system of reference is the one where X is at rest, as shown in Figures 5.2b, 5.2d. On the other hand, flight distances for the scalar boson X in the CMS frame have great values for $m_X = 50$ GeV as it is more boosted because of having a greater mass splitting between H and X bosons. In simple words, the main difference and the reason for the acceptance being smaller for `Sample 3`, lies in its mass splitting, where it is observed higher flight distances due to relativistic effects of time dilation in the CMS.

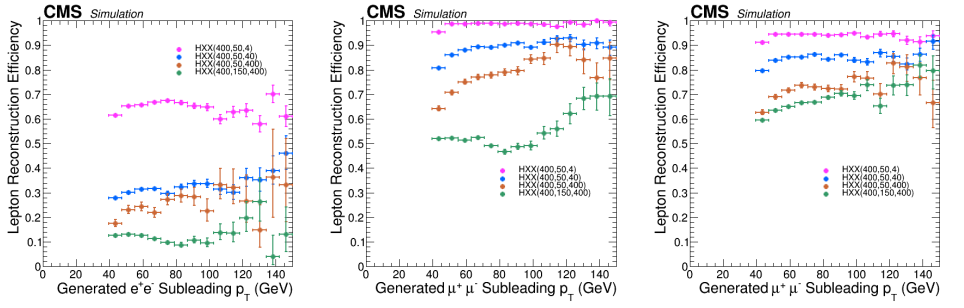

(A) Electron Reconstruction (B) Muon Reconstruction (C) Displaced Global Muon Reconstruction

FIGURE 5.3: Efficiencies for selecting two lepton (dilepton) candidates (dielectrons and dimuons) that satisfies selection requirements as function of transverse momentum p_T

The lepton reconstruction efficiency is defined for a pair of leptons fulfilling generated acceptance criteria in 5.1, which are correctly classified as reconstructed by CMS. The denominator represents a $X \to 2e(2\mu)$ candidate at generator level that fulfills criteria 5.1, whilst the numerator requires a $X \to 2e(2\mu)$ candidate at reconstruction level passing the acceptance criteria together with baseline requirements. Figures 5.3, 5.4, 5.5 show efficiencies for selecting two leptons candidates coming from a long-lived particle X with respect to transverse momenta p_T of subleading lepton, leading lepton pseudorapidity η and transverse decay length L_{xy} corresponding to the dilepton mother particle, respectively. All this quantities are evaluated at generation level. Additionally, for each figure it is shown efficiencies for both electron and muon channels, including DGM reconstruction for muons.

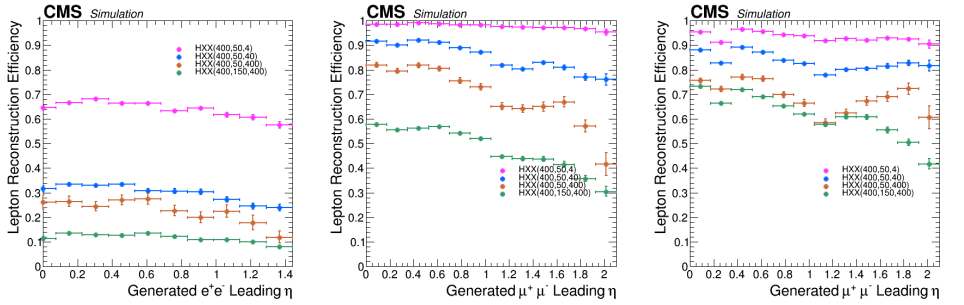

(A) Electron Reconstruction (B) Muon Reconstruction (C) Displaced Global Muon Reconstruction

FIGURE 5.4: Efficiencies for selecting two lepton (dilepton) candidates (dielectrons and dimuons) that satisfies selection requirements as function of pseudorapidity η

As shown in Figure 5.3a, the efficiency for electrons is flat for $p_T < 100$ GeV, beyond that value and in particular, for samples with higher $c\tau$, it is observed greater fluctuations in p_T since there are less events to fill efficiencies available. On the other hand, efficiencies for muon channel, illustrated in Figure 5.3b and Figure 5.4b, are higher ($\sim 100\%(MR1)$, $\sim 95\%(DGM)$ for `Sample 1`) in contrast to the efficiency obtained for electrons ($\sim 65\%$ for `Sample 1`); this is due to the fact electrons lose more energy than muons in their passage through the detector, making its reconstruction harder than for muons. For both MR1 and DGM, efficiencies as function of p_T and

η are relatively flat with a small decreasing area near the p_T minimum cut (40 GeV) and also, for high values of η ($\eta > 1$), where this behavior is more significant for MR1 than DGM. In general, MR1 and DGM efficiencies present a similar behavior with the exception for `Sample 4`,where there is an improvement for the DGM algorithm, since for MR1 efficiency is around $\sim$ 60% for $|\eta| < 1$ and for DGM is $\sim$ 75%.

Electron reconstruction according to its decay length L_{xy} in Figure 5.5a indicates as well a low efficiency for Samples with $c\tau = 400$ mm, with an important drop off for approximately $L_{xy} > 1$ cm for all samples. On the other side, efficiencies as a function of the transverse decay length L_{xy} show a good reconstruction for both old muon definition (MR1) (see Figure 5.5b) and new muon definition (DGM) (Figure 5.5c) til approximately 5 cm for `Samples 1, 2, 3`, where there is a drop off for both efficiencies as L_{xy} increases.

For instance, for `Sample 2` ($m_X = 50GeV$, $c\tau = 40mm$), MR1 reconstruction efficiency is around $\sim$ 100% for $L_{xy} < 5$ cm and it decreases steadily as it goes beyond that value; similarly to DGM reconstruction efficiency although its efficiency is around $\sim$ 95%. In contrast for `Sample 4` which kinematics is different from the other samples, the reconstruction efficiency for MR1 drops off for values of $L_{xy} > 2$ cm and for DGM, it starts to decrease steadily for $L_{xy} > 3$ cm. This means that DGM seems to improve the reconstruction for samples with high displaced $c\tau$ and also, it presents a slower decrease of efficiency as L_{xy} increases, in contrast to MR1. Such behavior is being consistent with the observed for p_T and η, since DGM efficiencies for `Sample 4` improved around $\sim$ 8% the reconstruction in comparison for MR1 efficiencies of such sample.

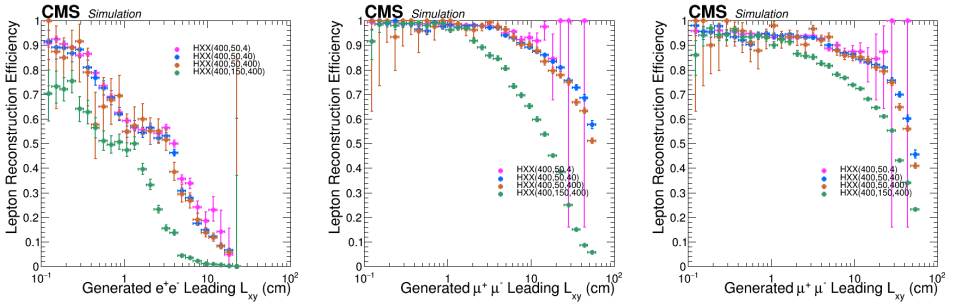

(A) Electron Reconstruction (B) Muon Reconstruction (C) Displaced Global Muon Reconstruction

FIGURE 5.5: Efficiencies for selecting two lepton (dilepton) candidates (dielectrons and dimuons) that satisfies selection requirements as function of transverse decay length L_{xy}

To summarize, as $c\tau$ starts to become larger, it starts to lose efficiency for reconstruction and the number of events where $X \to l^+l^-$ with p_T, η, L_{xy} cuts gets significant reduced (see acceptances after L_{xy} cut for `Samples 3,4` in Table 5.3). Nevertheless, as new algorithms for reconstruct displaced leptons are implemented, it can lead to higher efficiency of reconstruction for those long-lived particles with $c\tau$ around 400 mm, as clearly observed for the case of Muon-Run1 reconstruction in comparison to Displaced Global Muon-Run2 reconstruction.

5.1.2 Secondary Vertex Reconstruction Efficiencies

Secondary vertex reconstruction efficiencies are necessary in order to estimate how well those pair of leptons already reconstructed are being classified as for coming from a displaced vertex. In particular, the denominator represents a $X \to 2e(2\mu)$

candidate at reconstruction level that satisfies acceptance and baseline criteria (*i.e* numerator for lepton reconstruction efficiencies) and the numerator, besides requiring the same as the denominator, it also requires a valid secondary vertex using reconstruction information.

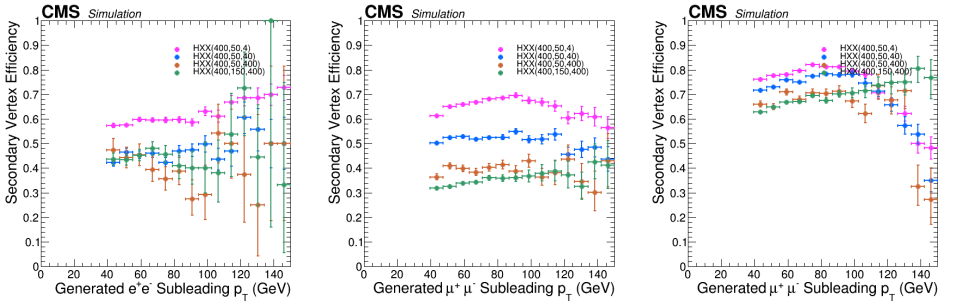

(A) Electron Reconstruction (B) Muon Reconstruction (C) Displaced Global Muon Reconstruction

FIGURE 5.6: Efficiencies for reconstructing a displaced dilepton (di-electron or dimuon) vertex that satisfies baseline selection as function of transverse momentum p_T

Figures 5.6, 5.7, 5.8 represent efficiencies for selecting dileptons coming from a valid displaced vertex as function of p_T, η, L_{xy}. The secondary vertex reconstruction for electrons with respect to p_T (Figure 5.6a) has an efficiency range between $40\% - 60\%$, where the lowest value corresponds to samples with $c\tau = 400$ mm and the highest corresponds to the sample with $c\tau = 4$ mm; and the efficiency with respect to η (Figure 5.7a) is quite flat and its values lie more or less in the same range. As for muons, the MR1 reconstruction (Figure 5.6b) shows a flat efficiency in a range of $30\% - 65\%$, the lowest corresponding to samples with $c\tau = 400$ mm and the highest to $c\tau = 4$ mm, this behavior is alike to the one with respect to η (Figure 5.7b). On the other hand, for the DGM it is observed an improvement in the efficiency with a range between $65\% - 85\%$ for p_T below than 100 GeV for the corresponding samples as illustrated in Figure 5.6c. As with respect to η, DGM reconstruction presents a quite steady and high efficiency around $68\% - 80\%$ for the samples, as shown in Figure 5.7c.

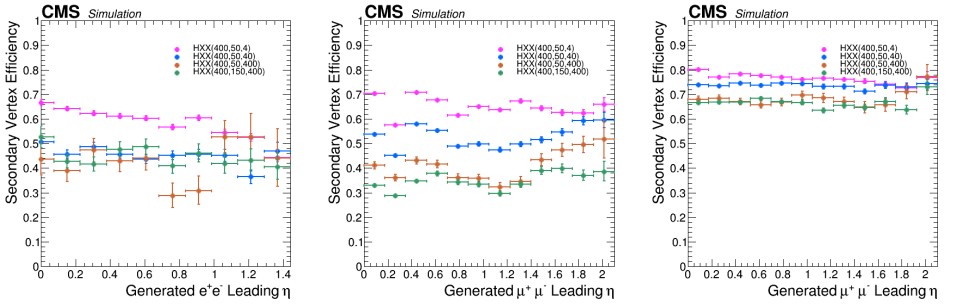

(A) Electron Reconstruction (B) Muon Reconstruction (C) Displaced Global Muon Reconstruction

FIGURE 5.7: Efficiencies for reconstructing a displaced dilepton (di-electron or dimuon) vertex that satisfies baseline selection as function of pseudorapidity η

To complement the former description, secondary vertex reconstruction with respect to L_{xy} shows a drop off around 2 cm for electrons for all the samples (see

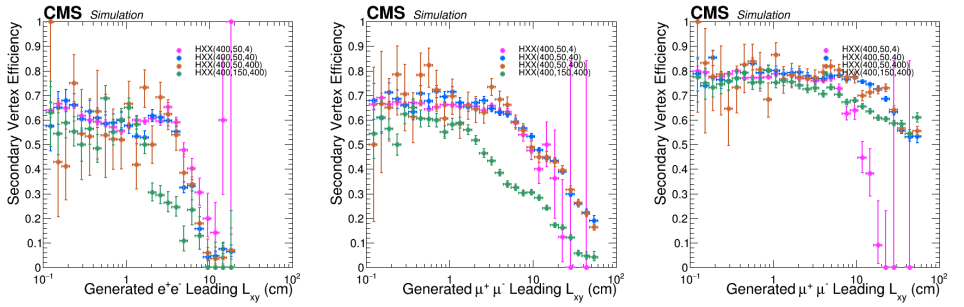

(A) Electron Reconstruction (B) Muon Reconstruction (C) Displaced Global Muon Reconstruction

FIGURE 5.8: Efficiencies for reconstructing a displaced dilepton (di-electron or dimuon) vertex that satisfies baseline selection as function of transverse decay length L_{xy}

Figure 5.8a) and around 6 cm for both MR1 and DGM reconstructions, as shown in Figure 5.8b and Figure 5.8c. However, for `Samples 1,2,3` the DGM reconstruction increases its efficiency around 7% and for `Sample 4` around 10% in comparison with MR1 secondary vertex efficiency.

As a result, the efficiency to correctly select dileptons coming from a displaced vertex as function of generated L_{xy} shows that the criteria for electrons is less efficient than for muons. In fact, DGM shows a better reconstruction in the whole L_{xy} range with smoother decreasing values of efficiency than MR1 reconstruction, especially from $2-5$ cm.

5.1.3 Total Efficiencies

In order to compare and give an overall estimation of the reconstruction efficiency for the long-lived particle of study, total efficiencies for lepton and secondary vertex reconstruction with respect to the transverse decay length L_{xy} for each sample is illustrated in the following figures.

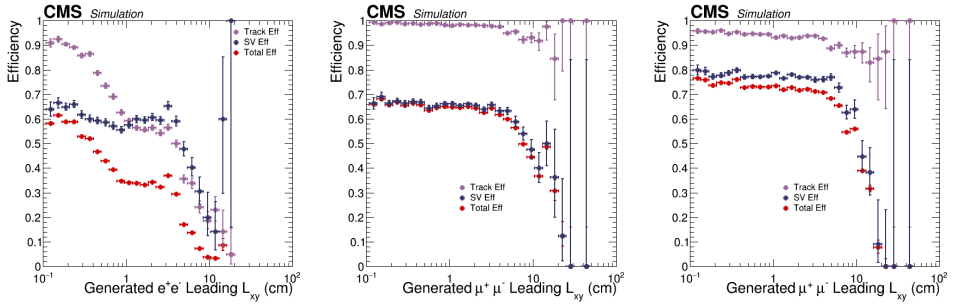

(A) Electron Reconstruction (B) Muon Reconstruction (C) Displaced Global Muon Reconstruction

FIGURE 5.9: Overall standard event reconstruction efficiency as function of transverse decay length L_{xy} for sample `50-4mm`

In general, `Samples 1,2,3` present an overall reconstruction efficiencies alike, where for X bosons decaying to electrons the efficiency of almost 60% decreases rapidly as L_{xy} increases and for muon channel, overall efficiencies present a plateau til values of L_{xy} of 5 cm for MR1 (65%) and 10 cm for DGM (75%), approximately. The main difference between efficiencies for `Samples 1,2,3` lies on their statistical

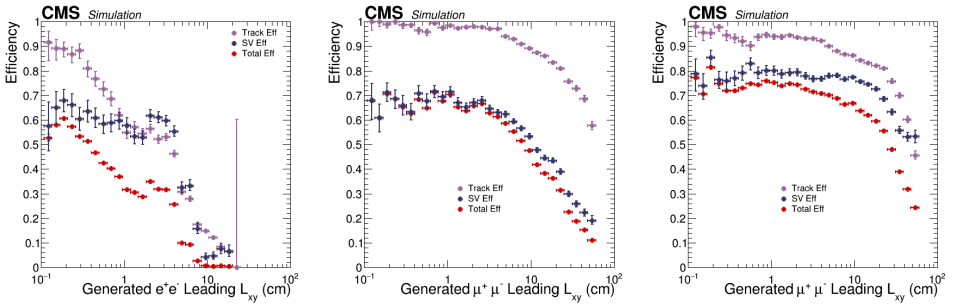

(A) Electron Reconstruction (B) Muon Reconstruction (C) Displaced Global Muon Reconstruction

FIGURE 5.10: Overall standard event reconstruction efficiency as function of transverse decay length L_{xy} for sample `50-40mm`

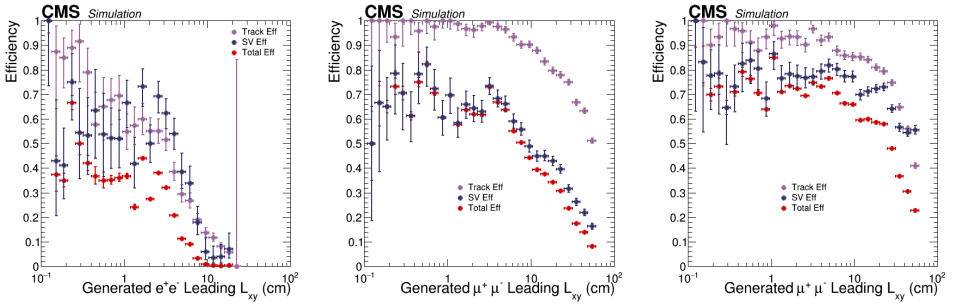

(A) Electron Reconstruction (B) Muon Reconstruction (C) Displaced Global Muon Reconstruction

FIGURE 5.11: Overall standard event reconstruction efficiency as function of transverse decay length L_{xy} for sample `50-400mm`

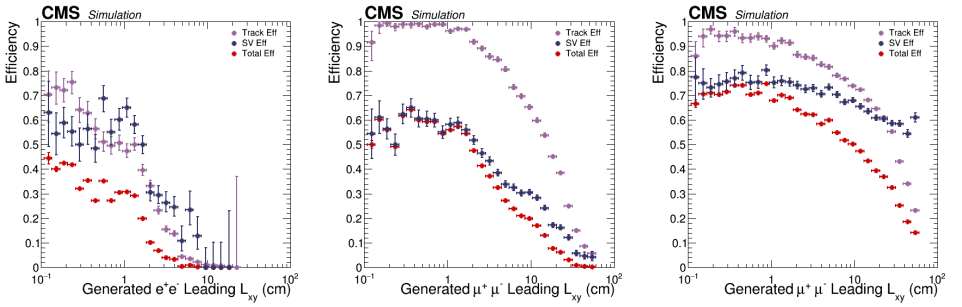

(A) Electron Reconstruction (B) Muon Reconstruction (C) Displaced Global Muon Reconstruction

FIGURE 5.12: Overall standard event reconstruction efficiency as function of transverse decay length L_{xy} for sample `150-400mm`

fluctuations as it is observed that for `Sample 1` there are less events to fill efficiencies for L_{xy} values greater than 10 cm, while for `Sample 3` fluctuations are found to be up until roughly 6 cm.

On the other hand, `Sample 2` presents a total efficiency with less statistical fluctuations in the overall spectra, meaning that there are enough statistics (events) in the whole range of L_{xy} that satisfied the conditions imposed to lepton and secondary vertex reconstruction, contrarily to `Samples 1,3`. Therefore, `Sample 2` provides a wide range of values for L_{xy} in which there is an event of interest, being an ideal efficiency description in the L_{xy} range studied.

5.2 Sensitivity and Optimization of Signal Cuts

As the motivation is the search for LLP, one goal is to show the experimental sensitivity for this kind of study as well as a way to optimize cuts that allow a fine-tuning of the signal for statistical significance. In that sense, reconstructed L_{xy} distributions for `Sample 1,2,3` and their respective figures of merit for the signal significance are shown in Figure 5.13 and Figure 5.14 and to simplify, the main two backgrounds here considered are *DY* and *ttbar*, since they are the most important[1].

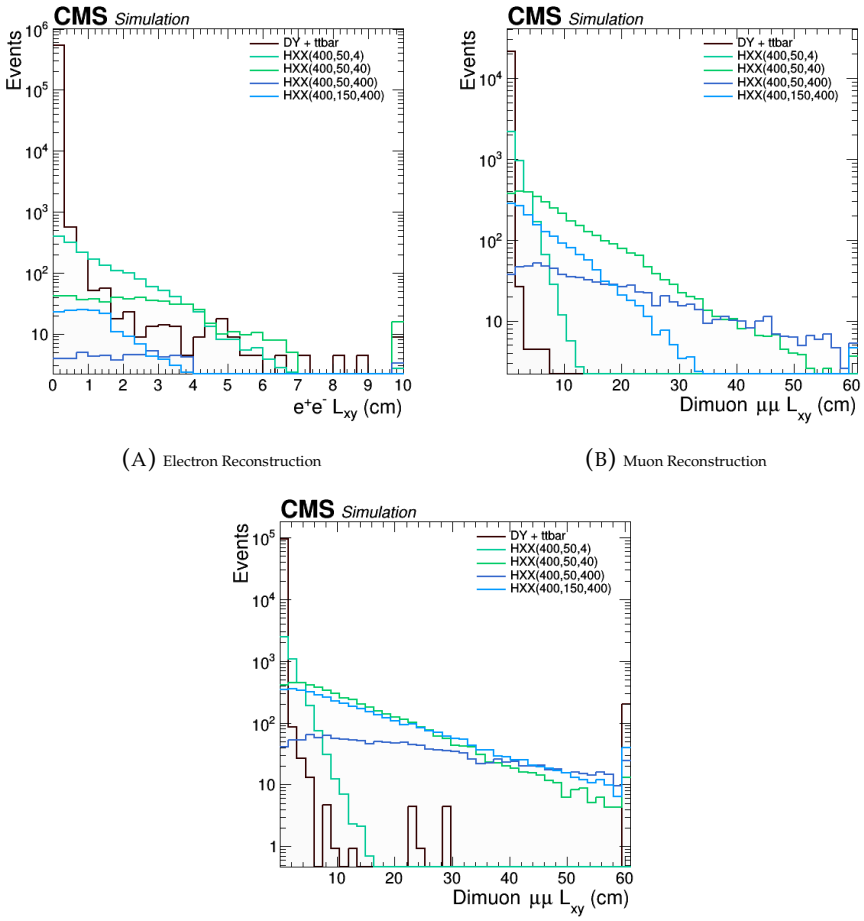

(A) Electron Reconstruction

(B) Muon Reconstruction

(C) Displaced Global Muon Reconstruction

FIGURE 5.13: The reconstructed L_{xy} distribution for electron (upper row) and muon (last two rows) channel for Muon-Run1 and DGM reconstruction.

The reconstructed L_{xy} distributions for both electron and muon channel are illustrated in Figure 5.13 for electron, MR1 and DGM reconstructions, respectively. In general, according to what it is observed in Figure 5.13, there is a well defined difference between background and signal for the muon channel, particularly for signal samples with the two highest values of $c\tau$, as shown for `Samples 2,3` in Figure 5.13b

[1] *DY* and *ttbar* are the main two background in SM containing high p_T dileptons with greater cross sections in the LHC.

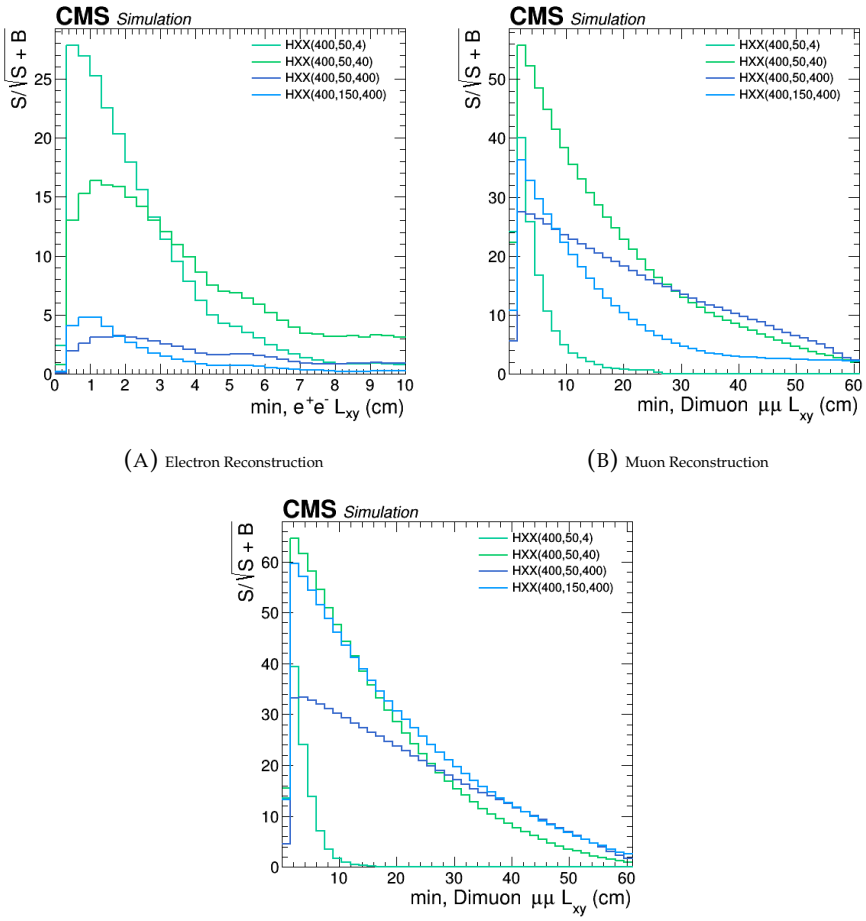

(A) Electron Reconstruction

(B) Muon Reconstruction

(C) Displaced Global Muon Reconstruction

FIGURE 5.14: Signal significance $S/\sqrt{S+B}$ for electron (upper row) and muon (last two rows) channel for Muon-Run1 and DGM reconstruction. S is the number of estimated events in the signal region and B is the number of estimated events in the control region.

for MR1 and Figures 5.13c for DGM. As for electrons, however, the difference between background and signal is not well defined and it is not as straightforward to see in which values of $c\tau$ is properly defined as in the case for muon channel.

In order to understand better and give a more qualitative signal analysis, Figure 5.14 illustrates a figure of merit widely used in high-energy physics that provides a way to exclude, search or find new signals and it is known as *Signal Significance*. In particular, the signal significance is here studied with respect to a selection criteria on the reconstructed L_{xy}. The expected number of events from signal(background) above a given L_{xy} value is denoted as $S(B)$. The signal significance is defined as $S/\sqrt{S+B}$ [74]. In other words, it allows to optimize a selection requirement on L_{xy} that provides the best trade-off between signal efficiency and background rejection for each sample in study.

In the muon channel, as shown in Figures 5.14b for MR1 and Figures 5.14c for DGM, signal significance is observed to have a higher value for the DGM reconstruction in contrast to the MR1, with the exception of `Sample 1` (teal curve), where

apparently for X bosons with shorter displacement $c\tau$, the significance is better for MR1 reconstruction. The statistical significance illustrated for the muon channel also suggests that an optimal cut to improve efficiency of reconstruction with respect to the reconstructed L_{xy} would be around $2-5$ cm. In addition, it is observed for `Sample 3` (blue curve) in Figure 5.14c that its signal significance decreases slowly, meaning that if a greater cut of L_{xy} is applied (*i.e* greater than $2-4$cm), signal significance is higher in comparison to samples with $c\tau$ of $4,40$ mm.

While for X bosons decaying to electrons, the signal significance is found to be higher for samples with lower $c\tau$, in other words, the lower the displacement of X boson, the better the sensitivity of the signal. However, the significance is quite low in comparison for the one obtained for muons. For instance, for `Sample 2` the signal significance is almost 4 times greater for muons than for electrons.

Additionally, other figures of merit commonly used in high-energy physics were implemented and considered for this analysis, such as $S/\sqrt{B}$ and $1.0/\sqrt{B}$, where the conclusions derived from them are the same as for $S/\sqrt{S+B}$.

5.3 Signal Estimation From Generator Level Information

The number of signal events in data, N_{signal}, can be described as the difference between the total number of dilepton events observed in data N and the number of estimated background events N_B; and it can be estimated by applying the expression for the signal cross section,

$$N_{signal} = \sigma_{(H\to XX)} \cdot \mathcal{L} \cdot \mathcal{A} \cdot \mathcal{E}_{selection} \tag{5.2}$$

where $\sigma_{(H\to XX)}$ is the cross section from the process, $\mathcal{L}$ is the integrated luminosity, $\mathcal{A}$ is the acceptance (as defined in criteria 5.1), $\mathcal{E}_{selection}$ is the efficiency of selection to reconstruct signal events within acceptance[2].

The standard method to obtained the number of signal events N_{signal} within the baseline selection from a given simulated sample is by means of eq. 5.2, using the values obtained for the acceptance $\mathcal{A}$ from generation level information (see Table 5.3) and the efficiency of selection $\mathcal{E}_{selection}$ is computed as the number of reconstructed events fulfilling the baseline selection over the total number of events in the sample.

On the other hand, the method here proposed is also based on eq. 5.2, although the efficiency of selection $\mathcal{E}_{selection}$ for a given $c\tau$ is computed exclusively from generation level information. Additionally, it is used reconstruction level information from a sample with $c\tau$ of reference to parameterize the reconstruction efficiency with respect to the generated L_{xy}, as mentioned in Subsection 5.1.3 for Figure 5.10. In this Subsection, it was found that the sample that better parameterize the efficiency is `Sample 2`, since it allows a better description in the whole range of L_{xy} without having many statistical fluctuations.

The simulation of particles through the detector is a complex process that requires several computing resources from the CMS experiment and, also, a demanding amount of computing time (weeks and even months), while the generated level information is a faster process, as briefly mentioned in Section 5.1. Hence, the main motivation of implementing this method is to provide an estimation of the number of signal events for a given $c\tau$, using only the generation level information for such

[2] In the present study, only signal events within the phase space corresponding to acceptance criteria are considered.

sample and reconstruction level for the parameterized sample of $c\tau$ in the intermediate range of interest[3], in order to save computing resources and time.

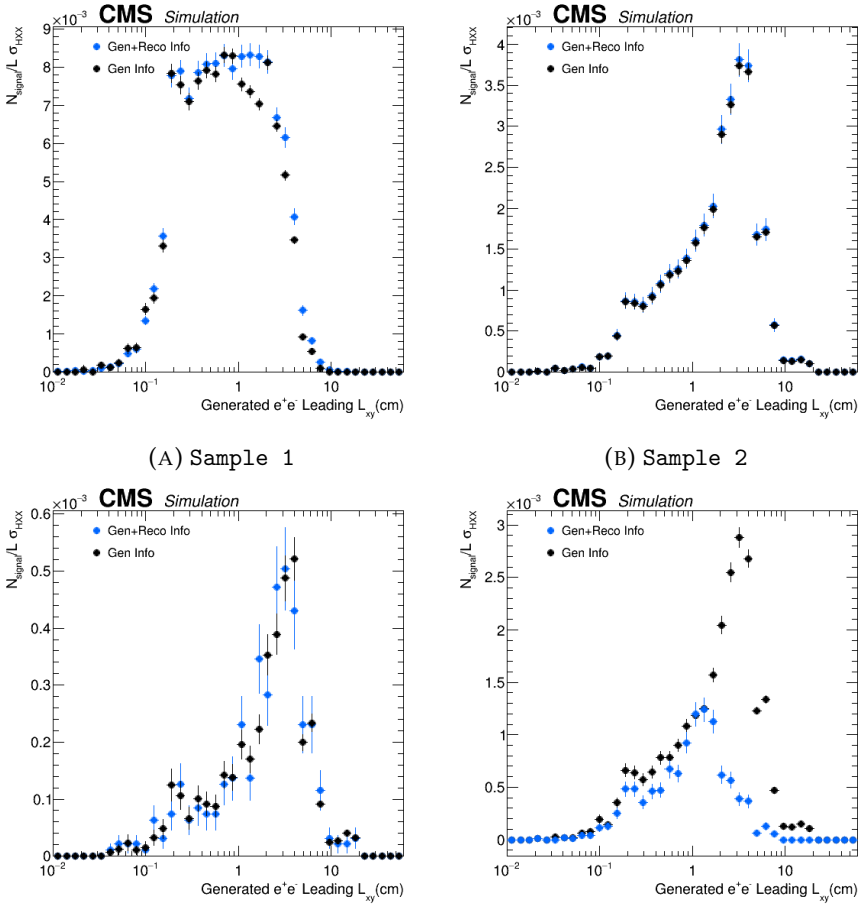

(A) `Sample 1` (B) `Sample 2`

(C) `Sample 3` (D) `Sample 4`

FIGURE 5.15: Number of signal events using the standard (blue) and proposed (black) methods as a function of the generated transverse decay length L_{xy}, when $X \rightarrow e^{-}e^{+}$. For the 2016 dataset at CMS, Luminosity is $\mathcal{L} = 39.5 fb^{-1}$ and cross section of $\sigma_{(H\rightarrow XX)} = 632.1 fb$ ($677.3 fb$ `Sample 4`) estimated by `PYTHIAv8`

Figures 5.15, 5.16, 5.17 illustrate the estimation of the number of signal events using the standard method (blue curve), meaning that the information used is at generated and reconstructed level, and using the proposed method (black), where it is used only generation level information for given $c\tau$.

For the electron channel, it is observed a reasonable agreement for the method proposed with the standard one for those samples with the same kinematics, such as `Samples 1,3` which values of $c\tau$ are 4, 400 mm, respectively (see for electron channel Figures 5.15a, 5.15c). However, for the sample with $c\tau$ of 4 mm, there is a weak disagreement for values of generated L_{xy} greater than 1 cm ($L_{xy} > 1$cm), this might

[3] An even more optimal choice for this purpose would be the usage of a (non-physical) simulated sample with a flat L_{xy} spectrum.

be caused by its abrupt behavior in the reconstruction efficiency around this range of L_{xy}, as illustrated in Figure 5.10a.

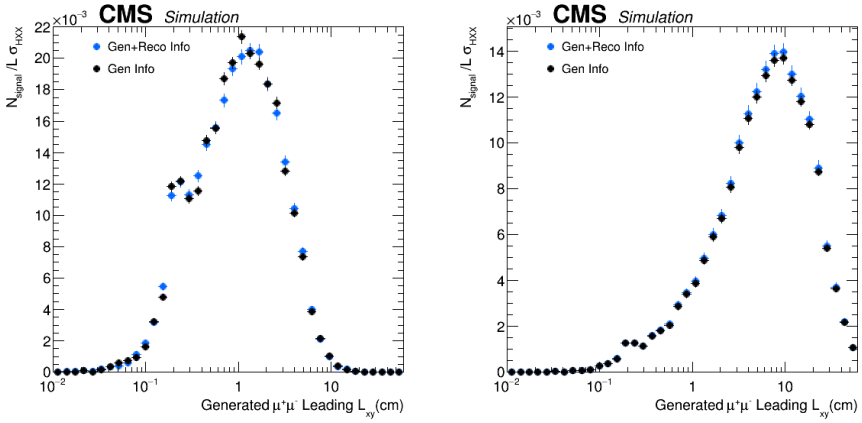

(A) `Sample 1` (B) `Sample 2`

(C) `Sample 3` (D) `Sample 4`

FIGURE 5.16: Number of signal events using the standard (blue) and proposed (black) methods as a function of the generated transverse decay length L_{xy}, when $X \rightarrow \mu^{-}\mu^{+}$ using the Muon-Run1 reconstruction algorithm. For the 2016 dataset at CMS, Luminosity is $\mathcal{L} = 39.5 fb^{-1}$ and cross section of $\sigma_{(H\rightarrow XX)} = 632.1 fb$ ($677.3 fb$ `Sample 4`) estimated by `PYTHIAv8`

On the other hand, for scalar bosons X decaying to muons, for `Samples 1,3` the model gives a good estimation of the number of signal events N_{signal}, as observed in Figures 5.16a and Figure 5.16b, where both distributions are compatible. It is important also to notice that for both cases (electron and muon) the estimation of N_{signal} is in good agreement between both methods used for `Sample 2`, as expected.

As for long-lived particles X with different kinematics as the case of the number of signal events for `Sample 4`, Figure 5.15d and Figure 5.16d show a significant discrepancy between both methods implemented. They are included to emphasize that the kinematics, such as different mass splitting between H and X and how boosted the X particle is, plays an important role to describe N_{signal} and thus, as it was expected, there is a bad agreement when trying to apply the efficiency based on `Sample 2` to the `Sample 4`.

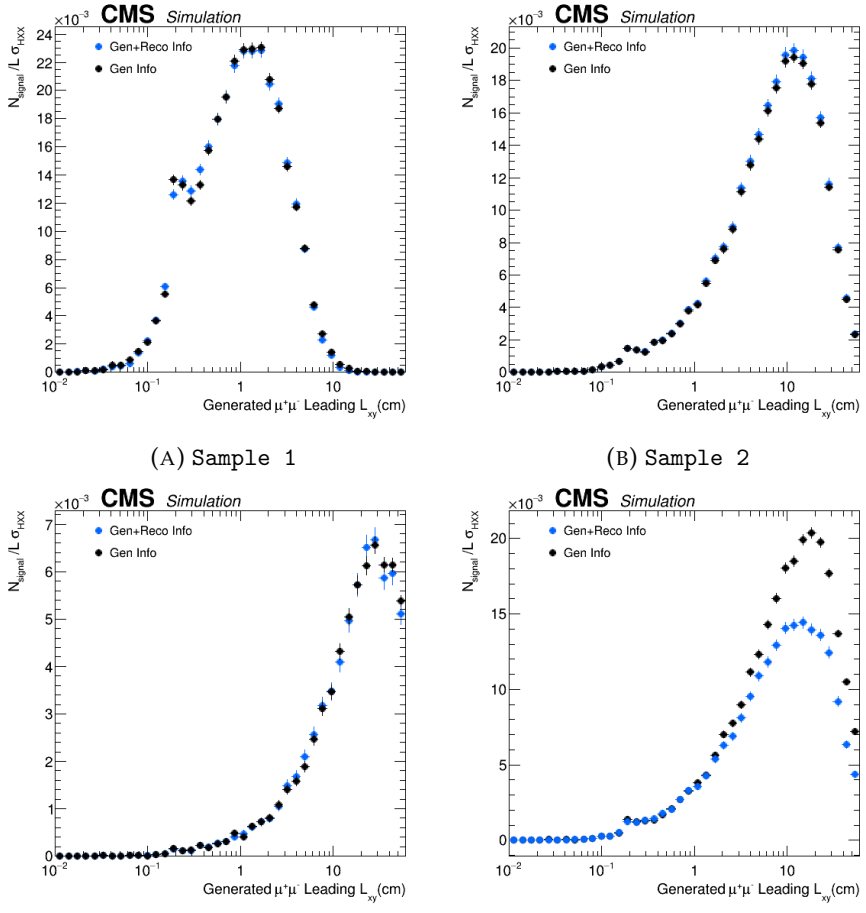

(A) `Sample 1` (B) `Sample 2`

(C) `Sample 3` (D) `Sample 4`

FIGURE 5.17: Number of signal events using the standard (blue) and proposed (black) methods as a function of the generated transverse decay length L_{xy}, when $X \to \mu^-\mu^+$ using the DGM-Run2 reconstruction algorithm. For the 2016 dataset at CMS, Luminosity is $\mathcal{L} = 39.5 fb^{-1}$ and cross section of $\sigma_{(H\to XX)} = 632.1 fb$ ($677.3 fb$ `Sample 4`) estimated by `PYTHIAv8`

The reconstruction of muons by DGM-Run2 offers a better estimation of N_{signal} for `Sample 4`, in contrast to MR1 reconstruction, as shown in Figure 5.17d. This is explained since DGM efficiency is probably less dependent on certain kinematic variables correlated to L_{xy} with respect to MR1 and electron reconstruction. As for samples with same kinematics (see Figures 5.17a, 5.17b, 5.17c), there is a good agreement, meaning that the proposed method provides a reasonable good approach to estimate the number of signal events for long-lived particles with same mass but different mean proper lifetimes that decay to final states containing dimuons, when generation level information is known.

5.3.1 Method for $XX \to 4e$ and $XX \to 4\mu$

For the present analysis, the final state considered for the scalar boson X is the one where one X decays to electrons and the other X decays to muons (BSM $H \to XX$,

$XX \rightarrow 2\mu 2e$)), being the interest of this analysis purely academic. However, this study could be extended to arbitrary values of the branching ratio BR, in order to be more realistic and thus, allowing to have a whole picture where X bosons decay either to $4e$ or to 4μ. The estimation of signal sensitivities for `Sample 2` is illustrated in Figure 5.18 for $XX \rightarrow 4e$ and Figure 5.19 for $XX \rightarrow 4\mu$, although a full study for the mentioned channels is beyond the scope of the present work.

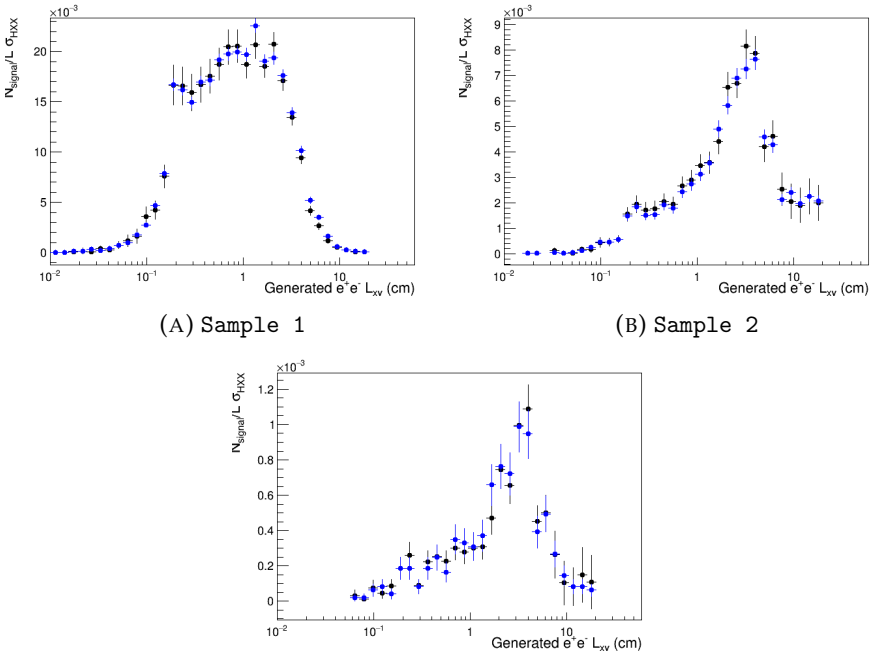

(A) `Sample 1` (B) `Sample 2`

(C) `Sample 3`

FIGURE 5.18: Number of signal events using the standard (blue) and proposed (black) methods as a function of the generated transverse decay length L_{xy}, when $X \rightarrow e^{-}e^{+}$. For the 2016 dataset at CMS, Luminosity is $\mathcal{L} = 39.5fb^{-1}$ and cross section of $\sigma_{(H \rightarrow XX)} = 632.1fb$ estimated by `PYTHIAv8`

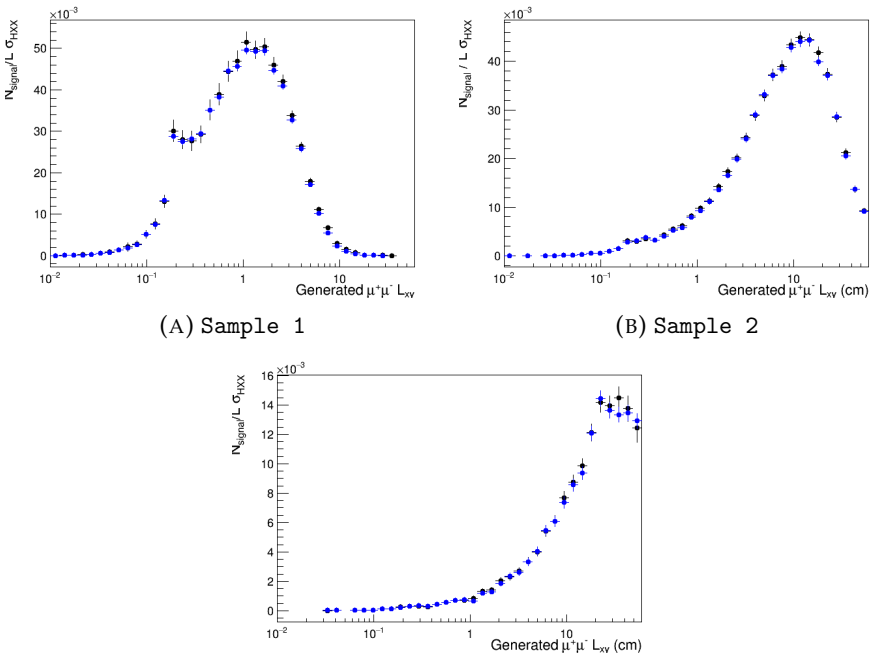

(A) `Sample 1` (B) `Sample 2`

(C) `Sample 3`

FIGURE 5.19: Number of signal events using the standard (blue) and proposed (black) methods as a function of the generated transverse decay length L_{xy}, when $X \rightarrow \mu^{-}\mu^{+}$. For the 2016 dataset at CMS, Luminosity is $\mathcal{L} = 39.5fb^{-1}$ and cross section of $\sigma_{(H\rightarrow XX)} = 632.1fb$ estimated by `PYTHIAv8`

Chapter 6

Summary & Concluding Remarks

This final master project presented a study based on an ongoing analysis of searches for long-lived particles that decay into final states containing displaced leptons in the Run 2 of the LHC, using 2016 data collected with the CMS detector in proton-proton collisions at $\sqrt{s} = 13$ TeV. The results given were obtained using simulated signal samples with `Pythia v8`, where they are interpreted in terms of a benchmark model that involves a BSM Higgs boson with mass of 400 GeV decaying into a pair of long-lived spinless bosons X in the mass range $50 - 150$ GeV, each of which decays back to dileptons (electrons and muons), with different mean proper decay lengths of the long-lived particles (LLP) in the range $4 - 400$ mm. The main purpose of the present final master project was to assess a model that estimates the number of signal events in a sample from information of generated LLP for a given $c\tau$ and to compare the performance between two muon reconstructions: Muon Run1-like (MR1) and Displaced Global Muon (DGM) Run 2-like algorithms.

The results obtained for lepton reconstruction show that as the mean decay length $c\tau$ of the long-lived X goes farther from the detector, it becomes harder to reconstruct and to properly identify dilepton candidates coming from bosons X. Similarly, for secondary vertex reconstruction, dileptons are associated to a valid displaced vertex with higher efficiency for those samples containing long-lived particles with shorter $c\tau$. However, it was showed an improvement for selecting signal events using the DGM reconstruction for samples highly displaced ($c\tau = 400$ mm) and, also it was showed that efficiencies for muons using DGM present a slow rate of decrease with respect to transverse decay length L_{xy}, in contrast to MR1. In addition, overall efficiencies with respect to generated transverse decay length L_{xy} were shown with the main purpose to compare the performance between MR1 and DGM reconstructions as well as to compare statistical fluctuations for each sample in study. In fact, the results obtained point out that there is an improvement of the performance of the DGM-Run2 over MR1 reconstruction, especially for samples with higher $c\tau$ and that a sample, with an intermediate value of $c\tau$ among different samples, represents better the whole range of L_{xy}, since it presents less statistical fluctuations around it. In short, such sample represents an ideal candidate to parameterize the reconstruction efficiency, as it provides a wide range of values for L_{xy} in which there is an event of interest.

Along with efficiencies, it was studied the signal significance for each sample, in order to optimize a selection requirement on L_{xy} that provides the best trade-off between signal efficiency and background rejection. It was found that for LLP decaying to muons, signal significance is higher when using DGM than MR1 and that samples with smaller $c\tau$ have a tight range of L_{xy} where there is signal. On the other hand, when decaying to electrons, the signal significance obtained is higher for samples with lower $c\tau$ in a tight range of L_{xy} than for more displaced samples,

although it is significantly lower than the signal significance obtained for muons. However, for highly displaced samples it was observed that its signal significance decreases at a slower rate than the others, meaning that it could be found more signal events when applying a stringent cut in L_{xy} in contrast to samples with low displacement.

Finally, it was proposed a method to estimate number of signal events in each sample using exclusively generation level information from each one, along with reconstruction information from an unique parameterized sample. The results obtained for muons show a good agreement between the number of signal events using the method proposed with the actual distribution using information at generator and reconstructed level (standard method), although an exception raised for samples with different kinematics (*i.e* different mass splitting between H and X bosons). However, when using DGM reconstruction the agreement between expected distributions of number of signal events improves significantly, as DGM efficiency is probably less dependent on certain kinematic variables correlated to L_{xy}. As for electron channel, it was observed for samples with kinematic alike a reasonable agreement with some weak discrepancy, which it might be caused by an abrupt behavior in the electron reconstruction efficiency. In general, the proposed method provided a reasonable good approach to estimate number of signal events in samples with same kinematics, when generation level information of each sample is known.

Bibliography

[1] CMS collaboration, CMS Collaboration, et al. "Search for long-lived particles decaying to final states that include dileptons". In: *CMS PAS EXO-12-037* (2014).

[2] PAM Dirac. "Proc. Roy. Soc." In: *A* 114 (1927), p. 243.

[3] Pascual Jordan and Wolfgang Pauli. "Zur Quantenelektrodynamik ladungsfreier Felder". In: *Zeitschrift für Physik* 47.3-4 (1928), pp. 151–173.

[4] Werner Heisenberg and Wolfgang Pauli. "Zur quantentheorie der wellenfelder. ii". In: *Zeitschrift für Physik* 59.3-4 (1930), pp. 168–190.

[5] Sheldon L Glashow. "Partial-symmetries of weak interactions". In: *Nuclear physics* 22.4 (1961), pp. 579–588.

[6] Steven Weinberg. "A model of leptons". In: *Physical review letters* 19.21 (1967), p. 1264.

[7] Abdus Salam and JC Ward. "Phys. Letters 13 (1964) 168; S. Weinberg". In: *Phys. Rev. Letters* 19.1264 (1967), p. 27.

[8] Martin M Block. *Neutrino interactions in the CERN heavy liquid bubble chamber*. Tech. rep. 1964.

[9] FJ Hasert et al. "Observation of neutrino-like interactions without muon or electron in the Gargamelle neutrino experiment". In: *Nuclear Physics B* 73.1 (1974), pp. 1–22.

[10] Michael E Peskin. "Beyond the standard model". In: *arXiv preprint hep-ph/9705479* (1997).

[11] Andrew Purcell. "Go on a particle quest at the first CERN webfest. Le premier webfest du CERN se lance à la conquête des particules". In: BUL-NA-2012-269. 35/2012 (2012), 10. URL: {https://cds.cern.ch/record/1473657}.

[12] Michael E Peskin. *Concepts of elementary particle physics*. Vol. 26. Oxford Master Series in Physic, 2019.

[13] Walter Greiner, Berndt Müller, et al. *Gauge theory of weak interactions*. Vol. 5. Springer, 1996.

[14] Peter W Higgs. "Broken symmetries and the masses of gauge bosons". In: *Physical Review Letters* 13.16 (1964), p. 508.

[15] Serguei Chatrchyan et al. "Observation of a new boson at a mass of 125 GeV with the CMS experiment at the LHC". In: *Physics Letters B* 716.1 (2012), pp. 30–61.

[16] Georges Aad et al. "Observation of a new particle in the search for the Standard Model Higgs boson with the ATLAS detector at the LHC". In: *Physics Letters B* 716.1 (2012), pp. 1–29.

[17] Lawrence Lee et al. "Collider searches for long-lived particles beyond the Standard Model". In: *Progress in Particle and Nuclear Physics* 106 (2019), pp. 210–255.

[18] Maarten C Brak. "The hierarchy problem in the standard model and little higgs theories". In: *Master's thesis, NIKHEF* (2004).

[19] Benjamin Grinstein. "A supersymmetric SU (5) gauge theory with no gauge hierarchy problem". In: *Nuclear Physics B* 206.3 (1982), pp. 387–396.

[20] David Curtin et al. "Long-lived particles at the energy frontier: the MATHUSLA physics case". In: *Reports on Progress in Physics* 82.11 (2019), p. 116201.

[21] Igor P Ivanov. "Building and testing models with extended Higgs sectors". In: *Progress in Particle and Nuclear Physics* 95 (2017), pp. 160–208.

[22] Juliette Alimena et al. "Searching for long-lived particles beyond the Standard Model at the Large Hadron Collider". In: *arXiv preprint arXiv:1903.04497* (2019).

[23] D de Florian et al. *arXiv: Handbook of LHC Higgs Cross Sections: 4. Deciphering the Nature of the Higgs Sector*. Tech. rep. 2016.

[24] David Curtin et al. "Exotic decays of the 125 GeV Higgs boson". In: *Physical Review D* 90.7 (2014). ISSN: 1550-2368. DOI: 10.1103/physrevd.90.075004. URL: http://dx.doi.org/10.1103/PhysRevD.90.075004.

[25] Juan Rodrigo Gonzalez Fernandez. "Study of processes with a pair of top-antitop quarks and missing transverse energy in the final state in proton-proton collisions with the CMS detector at the Run 2 of the LHC". PhD thesis. Oviedo U., 2019.

[26] Rémi Barbier et al. "R-parity-violating supersymmetry". In: *Physics reports* 420.1-6 (2005), pp. 1–195.

[27] Lillian Hoddeson et al. *The rise of the standard model: A history of particle physics from 1964 to 1979*. Cambridge University Press, 1997.

[28] Chris Llewellyn Smith. "Genesis of the Large Hadron Collider". In: *Philosophical Transactions of the Royal Society A: Mathematical, Physical and Engineering Sciences* 373.2032 (2015), p. 20140037.

[29] Lyndon Evans and Philip Bryant. "LHC machine". In: *Journal of instrumentation* 3.08 (2008), S08001.

[30] Thomas Sven Pettersson, P Lefevre, LHC Study Group, et al. "The Large Hadron collider: conceptual design". In: *CERN, Geneva, Tech. Rep. CERN-AC-95-05 LHC* (1995).

[31] Kenneth Aamodt et al. "The ALICE experiment at the CERN LHC". In: *Journal of Instrumentation* 3.08 (2008), S08002.

[32] CMS Collaboration et al. *The CMS experiment at the CERN LHC*. 2008.

[33] A Augusto Alves Jr et al. "The LHCb detector at the LHC". In: *Journal of instrumentation* 3.08 (2008), S08005.

[34] ATLAS collaboration et al. *The ATLAS experiment at the CERN large hadron collider, 2008*. 2008.

[35] Christiane Lefèvre. "The CERN accelerator complex. Complexe des accélérateurs du CERN". 2008. URL: {http://cds.cern.ch/record/1260465}.

[36] G. L. Bayatian et al. "CMS Physics: Technical Design Report Volume 1: Detector Performance and Software". In: (2006).

[37] Tai Sakuma and Thomas McCauley. "Detector and Event Visualization with SketchUp at the CMS Experiment". In: *Journal of Physics: Conference Series* 513.2 (2014), p. 022032. DOI: 10.1088/1742-6596/513/2/022032. URL: https://doi.org/10.1088%2F1742-6596%2F513%2F2%2F022032.

[38] John R Hubbard. "LHC trigger design". In: (1997).

[39] Albert M Sirunyan, CMS collaboration, et al. "Particle-flow reconstruction and global event description with the CMS detector". In: *JINST* 12.10 (2017), P10003.

[40] Hale Sert. *CMS High Level Trigger Performance in Run 2*. Tech. rep. CMS-CR-2019-278. Geneva: CERN, 2019. URL: {https://cds.cern.ch/record/2712275}.

[41] CMS collaboration et al. "The CMS trigger system". In: *arXiv preprint arXiv:1609.02366* (2016).

[42] Giovanni Franzoni, Compact Muon Solenoid Collaboration, et al. "Dataset definition for CMS operations and physics analyses". In: *Nuclear and particle physics proceedings* 273 (2016), pp. 929–933.

[43] S. Mrenna T. Sjostrand and P.Z. Skands. "PYTHIA 6.4 physics and manual". In: *JHEP* 06 (2006). URL: doi:10.1088/1126-6708/2006/05/026,Arvix:hep-ph/0603175.

[44] C. Oleari S. Alioli P. Nason and E. Re. "A general framework for implementing NLO calculations in shower Monte Carlo programs: the POWHEG BOX". In: *JHEP* 06 (2010). URL: doi:10.1007/JHEP06(2010)043,Arvix:1002.2581.

[45] et al J Alwall. "The automated computation of tree-level and next-to-leading order differential cross sections, and their matching to parton shower simulations". In: *JHEP* 07 (2014). URL: doi:10.1007/JHEP07(2014)079,Arvix:1002.2581.

[46] GEANT4 Collaboration. "GEANT4 a simulation toolkit". In: *Instum.Meth* A506 (2003). URL: doi:10.1016/S0168-9002(03)01368-8,Arvix:1002.2581.

[47] Devis Contarato. *Silicon detectors for particle tracking at future high-energy physics experiments*. Tech. rep. 2005.

[48] *Modern particle physics*. Chap. 1. Introduction.

[49] CMS collaboration et al. "Description and performance of track and primary-vertex reconstruction with the CMS tracker". In: *Journal of Instrumentation* 9.10 (2014), P10009.

[50] Alessandro Caratelli. *Research and development of an intelligent particle tracker detector electronic system*. Tech. rep. EPFL, 2019.

[51] W Adam et al. "Reconstruction of electrons with the Gaussian-sum filter in the CMS tracker at the LHC". In: *Journal of Physics G: Nuclear and Particle Physics* 31.9 (2005), N9–N20. DOI: 10.1088/0954-3899/31/9/n01. URL: https://doi.org/10.1088%2F0954-3899%2F31%2F9%2Fn01.

[52] Nicolo Trevisani. "Search for Dark Matter produced in association with a Higgs boson in the WW fully leptonic decay channel in pp collisions at ssqrt13 TeV at the LHC with the CMS detector". PhD thesis. Cantabria U., Santander, 2019.

[53] S. Chatrchyan et al. "Performance and Operation of the CMS Electromagnetic Calorimeter". In: *Journal of Instrumentation* 5 (Jan. 2010).

[54] Werner Lustermann et al. "The electromagnetic calorimeter of cms, summary and status". In: *Journal of Physics: Conference Series*. Vol. 160. 1. IOP Publishing. 2009, p. 012044.

[55] Emilio Meschi et al. *Electron Reconstruction in the CMS Electromagnetic Calorimeter*. Tech. rep. CMS-NOTE-2001-034. Geneva: CERN, 2001. URL: {https://cds.cern.ch/record/687345}.

[56] Pierluigi Paolucci. *The CMS Muon system*. Tech. rep. CMS-CR-2006-006. Geneva: CERN, 2005. DOI: {10.1142/9789812773678_0096}. URL: {https://cds.cern.ch/record/927394}.

[57] Florian Beaudette. "The CMS particle flow algorithm". In: *arXiv preprint arXiv:1401.8155* (2014).

[58] Eric James et al. *Muon identification in CMS*. Tech. rep. CERN-CMS-NOTE-2006-010, 2006.

[59] CMS collaboration et al. "Performance of the CMS muon detector and muon reconstruction with proton-proton collisions at s= 13 TeV". In: *Journal of Instrumentation* 13.6 (2018), P06015.

[60] T. Speer et al. "Track reconstruction in the CMS tracker". In: *Nuclear Instruments and Methods in Physics Research Section A: Accelerators, Spectrometers, Detectors and Associated Equipment* 559.1 (2006). Proceedings of the X International Workshop on Advanced Computing and Analysis Techniques in Physics Research, pp. 143 –147. ISSN: 0168-9002. DOI: https://doi.org/10.1016/j.nima.2005.11.207.

[61] CMS Collaboration et al. "Technical Design Report, Volume I: Detector Performance and Software". In: *CMS Physics* (2006).

[62] CMS collaboration et al. "Muon reconstruction and identification improvements for run-2 and first results with 2015 run data". In: *CMS Detector Performance Summary CMS-DP-15-015* (2015).

[63] CMS collaboration et al. "Performance of CMS muon reconstruction in cosmic-ray events". In: *Journal of Instrumentation* 5.03 (2010), T03022.

[64] CMS collaboration et al. "Muon reconstruction and identification improvements for run-2 and first results with 2015 run data". In: *CMS Detector Performance Summaries CERN-CMS-DP-2015-015* 1 (2015), p. 15.

[65] "Performance of electron reconstruction and selection with the CMS detector in proton-proton collisions at sqrt(s)= 8 TeV". In: *Journal of Instrumentation* 10.06 (2015), P06005–P06005. DOI: 10.1088/1748-0221/10/06/p06005. URL: https://doi.org/10.1088%2F1748-0221%2F10%2F06%2Fp06005.

[66] Albert M Sirunyan et al. "Measurements of Higgs boson properties in the diphoton decay channel in proton-proton collisions at sqrt(s)= 13 TeV". In: *Journal of High Energy Physics* 2018.11 (2018), p. 185.

[67] "Performance of photon reconstruction and identification with the CMS detector in proton-proton collisions at sqrt= 8 TeV". In: *Journal of Instrumentation* 10.08 (2015), P08010–P08010. DOI: 10.1088/1748-0221/10/08/p08010. URL: https://doi.org/10.1088%2F1748-0221%2F10%2F08%2Fp08010.

[68] Rudolf Fruehwirth et al. "New vertex reconstruction algorithms for CMS". In: *arXiv preprint physics/0306012* (2003).

[69] Wolfgang Waltenberger, Rudolf Fruehwirth, and Pascal Vanlaer. "Adaptive vertex fitting". In: *Journal of Physics G: Nuclear and Particle Physics* 34.12 (2007), N343.

[70] Wolfgang Adam. "Track and vertex reconstruction in CMS". In: *Nuclear Instruments and Methods in Physics Research Section A: Accelerators, Spectrometers, Detectors and Associated Equipment* 582.3 (2007). VERTEX 2006, pp. 781 –784. ISSN: 0168-9002. DOI: https://doi.org/10.1016/j.nima.2007.07.091.

[71] Thomas Speer et al. *Vertex fitting in the CMS tracker*. Tech. rep. CERN-CMS-NOTE-2006-032, 2006.

[72] CMS collaboration et al. "Identification of b-quark jets with the CMS experiment". In: *Journal of Instrumentation* 8.04 (2013), P04013.

[73] et.al CF Madrazo. "Search for long-lived particles decaying to final states that include a displaced dilepton vertex". unpublished, Long-Lived Exotica WG Meeting on X-XX leptonic analyses. 2019.

[74] P.A. Zyla et al. "(Particle Data Group), Prog. Theor. Exp. Phys." In: (2020). 083C01.